
Article:
O'Regan, L., Barone, G., Adib, R. et al. (10 more authors) (2020) EML4-ALK V3 oncogenic fusion proteins promote microtubule stabilization and accelerated migration through NEK9 and NEK7. Journal of Cell Science, 133 (9). jcs.241505. ISSN 0021-9533

https://doi.org/10.1242/jcs.241505

EML4-ALK V3 oncogenic fusion proteins promote microtubule stabilization and accelerated migration through NEK9 and NEK7

Laura O'Regan[1,8*], Giancarlo Barone[1,2*], Rozita Adib[1], Chang Gok Woo[3], Hui Jeong Jeong[4], Emily L. Richardson[1], Mark W. Richards[5], Patricia A.J. Muller[6], Spencer J. Collis[2], Dean A. Fennell[7], Jene Choi[4], Richard Bayliss[5] and Andrew M. Fry[1,8]

[1]Department of Molecular and Cell Biology, University of Leicester, Lancaster Road, Leicester LE1 9HN, U.K.

[2]Department of Oncology and Metabolism, Sheffield Institute for Nucleic Acids (SInFoNiA), University of Sheffield, Beech Hill Road, Sheffield S10 2RX, U.K.

[3]Department of Pathology, Chungbuk National University Hospital, Chungbuk National University College of Medicine, Cheongju, Korea.

[4]Department of Pathology, Asan Medical Center, University of Ulsan College of Medicine, Seoul, Korea.

[5]School of Molecular and Cellular Biology, Astbury Centre for Structural Molecular Biology, Faculty of Biological Sciences, University of Leeds, Leeds LS2 9JT, U.K.

[6]Cancer Research UK Manchester Institute, University of Manchester, Alderley Park SK10 4TG, U.K.

[7]Cancer Research Centre, University of Leicester, Robert Kilpatrick Clinical Sciences Building, Leicester LE1 9HN, U.K.

[8]To whom correspondence should be addressed:

L.O.: tel: +44 116 229 7069; fax: +44 116 229 7018; email: lo29@le.ac.uk

A.M.F.: tel: +44 116 229 7069; fax: +44 116 229 7018; email: amf5@le.ac.uk

*These authors made equal contributions

JCS Advance Online Article. Posted on 17 March 2020

SUMMARY

EML4-ALK is an oncogenic fusion present in ~5% non-small cell lung cancers. However, alternative breakpoints in the *EML4* gene lead to distinct variants with different patient outcomes. Here, we show in cell models that EML4-ALK variant 3 (V3), which is linked to accelerated metastatic spread, causes microtubule stabilization, formation of extended cytoplasmic protrusions and increased cell migration. It also recruits the NEK9 and NEK7 kinase to microtubules via the N-terminal EML4 microtubule-binding region. Overexpression of wild-type EML4 as well as constitutive activation of NEK9 also perturb cell morphology and accelerate migration in a microtubule-dependent manner that requires the downstream kinase NEK7 but not ALK activity. Strikingly, elevated NEK9 expression is associated with reduced progression-free survival in EML4-ALK patients. Hence, we propose that EML4-ALK V3 promotes microtubule stabilization through NEK9 and NEK7 leading to increased cell migration. This represents a novel actionable pathway that could drive metastatic disease progression in EML4-ALK lung cancer.

KEYWORDS

EML4-ALK; EML4; NEK9; NEK7; NSCLC; microtubules; cell migration; metastasis

INTRODUCTION

The EML4-ALK translocation is an oncogenic driver in a subset of lung cancers resulting from an inversion on the short arm of chromosome 2. This creates an in-frame fusion of an N-terminal fragment of the echinoderm microtubule-associated protein-like 4, EML4 (Li and Suprenant, 1994; Suprenant et al., 1993), to the C-terminal tyrosine kinase domain of the anaplastic lymphoma kinase, ALK. The fusion was first identified in non-small-cell lung cancer (NSCLC), where it is present in ~5% of cases, but has since been identified in other tumour types, including breast and colorectal cancers (Lin et al., 2009; Rikova et al., 2007; Soda et al., 2007). The majority of EML4-ALK lung cancers, respond remarkably well to catalytic inhibitors of the ALK tyrosine kinase, such as crizotinib. However, this approach is not curative as acquired resistance to ALK inhibitors is inevitable due to either secondary mutations in the ALK tyrosine kinase domain or off-target alterations that switch dependence to other signalling pathways (Choi et al., 2010; Crystal et al., 2014; Hrustanovic et al., 2015; Kwak et al., 2010; McCoach et al., 2018; Shaw et al., 2013). Consequently, alternative therapies capable of selectively targeting ALK inhibitor resistant lung cancers are warranted.

It is clear that not all EML4-ALK patients respond well to ALK inhibitors in the first place (Woo et al., 2017). One potential explanation is the presence of alternative EML4-ALK variants that arise from distinct breakpoints (Bayliss et al., 2016; Choi et al., 2008). All fusions encode the C-terminal catalytic domain of the ALK kinase and an N-terminal coiled-coil from EML4 that promotes oligomerization and autophosphorylation. However, alternative breakpoints in the *EML4* gene lead to variable amounts of EML4 being present in the fusions. The N-terminal coiled-coil of EML4 (residues 14-63) has been shown by X-ray crystallography to form trimers (Richards et al., 2015). This sequence is followed by an unstructured region of approximately 150 residues rich in serine, threonine and basic residues. Based on crystallographic analysis of the related EML1 protein, the ~600 residue C-terminal region of EML4 (residues 216-865) is predicted to fold into a tandem pair of atypical β-propellers termed the TAPE domain (Richards et al., 2014). Structure-function studies have shown that while the C-terminal TAPE domain binds to α/β-tubulin heterodimers, it is the N-terminal domain (NTD) encompassing the coiled-coil and unstructured region that promotes binding to polymerized microtubules (Richards et al., 2014; Richards et al., 2015).

While all EML4-ALK fusion proteins have the trimerization motif, the distinct breakpoints mean that the different variants encode more or less of the unstructured and TAPE domains. Thus, the longer variants, V1 and V2, encode the unstructured domain and a partial fragment of the TAPE domain, while the shorter variants, V3 and V5, have none of the TAPE domain. Interestingly, the presence of a TAPE domain fragment renders the V1 and V2 fusion proteins unstable and dependent on the HSP90 chaperone for expression (Heuckmann et al., 2012;

Richards et al., 2014). Indeed, binding to HSP90 may interfere with microtubule association as these longer variants localise poorly to the microtubule network despite containing the microtubule-binding region (Richards et al., 2015). In theory, this identifies an alternative therapeutic approach for patients with the longer variants through use of HSP90 inhibitors, although to date clinical trials of HSP90 inhibitors have not shown efficacy in ALK-positive patients (Chatterjee et al., 2016; Chen et al., 2010; Workman and van Montfort, 2014). Moreover, HSP90 inhibitors would not be useful in patients with EML4-ALK V3 or V5 as these fusion proteins are not dependent upon HSP90 for their expression. Furthermore, patients with V3 respond less well to ALK inhibitors suggesting additional tumorigenic mechanisms that may be independent of ALK activity (Woo et al., 2017). This is important as V3 represents up to 50% of EML4-ALK fusions in NSCLC (Choi et al., 2010; Choi et al., 2008; Christopoulos et al., 2018; Sasaki et al., 2010; Woo et al., 2017).

Wild-type EML proteins have been found to interact with members of the human NEK kinase family (Ewing et al., 2007). The human genome encodes eleven NEKs, named NEK1 to NEK11, many of which exhibit cell cycle-dependent activity and have functions in microtubule organization (Fry et al., 2017; Fry et al., 2012; Moniz et al., 2011). NEK9, NEK6 and NEK7 are activated in mitosis and act together to regulate mitotic spindle assembly with NEK9 upstream of NEK6 and NEK7 (Sdelci et al., 2011). NEK6 and NEK7 are the shortest of the NEKs consisting solely of a kinase domain with a short N-terminal extension that determines their substrate specificity (de Souza et al., 2014; Vaz Meirelles et al., 2010). Moreover, they are ~85% identical within their catalytic domains. NEK9 is one of the longest NEKs, consisting of an N-terminal catalytic domain (residues 52-308) followed by a C-terminal regulatory region (residues 309-979). Within this C-terminal region is an RCC1 (regulator of chromatin condensation 1)-like domain (residues 347-726) that is predicted to fold into a seven-bladed β-propeller. Biochemical studies indicate that deletion of the RCC1-like domain causes constitutive activation of NEK9, indicating that it acts as an auto-inhibitory domain (Roig et al., 2002). This domain is followed by a C-terminal tail that contains a coiled-coil motif (residues 891-939) that promotes NEK9 dimerization (Roig et al., 2002). NEK9 directly interacts with NEK7, and presumably NEK6, through a short sequence (residues 810-828) that lies between the RCC1-like domain and coiled-coil (Haq et al., 2015). NEK9 stimulates NEK6 and NEK7 kinase activity by multiple mechanisms, including activation loop phosphorylation, dimerization-induced autophosphorylation, and allosteric binding-induced reorganization of catalytic site residues (Belham et al., 2003; Haq et al., 2015; Richards et al., 2009).

Here, we demonstrate that expression of not only activated NEK9 and NEK7 kinases but also full-length EML4 and the short EML4-ALK variants that bind microtubules (V3 and V5) alter cell morphology and promote cell migration. These changes are not seen in cells expressing the longer variants (V1 and V2) that do not bind microtubules. Moreover, our data reveal

interaction between the EML4 NTD and NEK9, and suggest a model in which the EML4-ALK V3 and V5 proteins stabilise microtubules and perturb cell behaviour through recruitment of NEK9 and NEK7 to microtubules. Finally, we show that EML4-ALK lung cancer patients exhibit a significant correlation between expression of V3/V5 and high levels of NEK9 protein, and that elevated NEK9 expression is associated with worse progression-free survival raising the prospect of novel therapeutic approaches for these patients.

RESULTS

Constitutively-active NEK9 alters interphase cell morphology and stabilises microtubules

We initially set out to explore the function of NEK9 by analysing the consequences of its untimely activation in interphase cells. For this, an inducible system was established in which expression of myc-tagged wild-type NEK9, a full-length kinase-inactive mutant (K81M), and a constitutively-activated mutant lacking the RCC1-like domain (ΔRCC1) was placed under the control of a tetracycline-inducible promoter in U2OS osteosarcoma cells (Fig. 1A). Western blots indicated time-dependent induction of expression of all three recombinant proteins upon addition of doxycycline, while subcellular localization confirmed the previously described cytoplasmic localization of the full-length and activated (ΔRCC1) proteins, and nuclear localization of the catalytically-inactive mutant (Roig et al., 2002) (Fig. 1B; and Supp. Fig. S1A). Flow cytometry indicated no significant change in cell cycle distribution upon induction of these NEK9 proteins (Supp. Fig. S1B). Unexpectedly, brightfield and immunofluorescence microscopy revealed that induction of activated NEK9 led to a change in interphase cell morphology with formation of long cytoplasmic protrusions that were not seen upon induction of either wild-type or catalytically-inactive NEK9 (Fig. 1C-E and Supp. Fig. S1C). Time-lapse imaging indicated that these protrusions were comparatively stable structures that did not undergo retraction except during cell division (Fig 1F). Depolymerisation of the microtubule network with nocodazole or vinorelbine caused loss of these protrusions indicating that they are microtubule-dependent (Fig. 1G), while super-resolution microscopy revealed that protrusions contained not only microtubules and the activated NEK9 protein, but also actin and acetylated tubulin (Fig. 1H, I). Western blotting confirmed that induction of activated NEK9 was associated with an increased overall expression of acetylated tubulin, a marker of stabilised microtubules (Fig. 1J). Consistent with this, time-lapse imaging of live cells incubated with the fluorescent SiR-tubulin probe (Lukinavicius et al., 2014) demonstrated that microtubules were more resistant to nocodazole-induced depolymerization following induction of the activated NEK9 kinase (Fig. 1K; and Supp. Fig. S1D). Hence, activation of NEK9 leads to a microtubule-dependent change in interphase cell morphology characterised by formation of elongated cytoplasmic protrusions that contain both actin and stabilised microtubules.

Activated NEK9 stimulates cell migration

Time-lapse imaging of cells expressing the activated NEK9 construct suggested that these cells not only underwent a change in morphology but also exhibited increased migration. To test whether activated NEK9 alters parameters of cell migration, the rate of closure of a scratch wound on 2D cell culture plates was measured. This revealed that cells induced to express the activated NEK9 closed the wound more quickly than cells containing an empty vector or cells containing the activated NEK9 construct but without induction (Fig. 2A, B). This did not appear to result from increased persistence in directional migration into the wound as these cells migrated with reduced straightness compared to control cells (Fig. 2C). Individual cell tracking experiments in sparsely plated cells confirmed a significant increase in the velocity of migration as well the distance travelled in isolated cells induced to express activated NEK9 (Fig. 2D-F). Furthermore, in the absence of a chemoattractant, there was a decrease in the straightness of migration in isolated cells in the presence of activated NEK9 consistent with more frequent changes in direction of migration (Fig. 2G). Finally, continuous monitoring of cell migration using a real-time transwell migration assay provided further evidence that induction of activated NEK9 led to an increased rate of migration; this was evident at 10 hours after induction and is therefore is not a result of increased proliferation (Fig. 2H, I). This assay measures 2D migration in response to serum suggesting that accelerated migration can occur in a directional manner in the presence of a chemoattractant as might be expected if growth factor receptors are expressed on the cytoplasmic protrusions. Taken together, these data demonstrate that activated NEK9 not only leads to a change in interphase cell morphology but also enhances cell migration.

NEK9-induced changes in cell morphology and migration are dependent on NEK7

A major function of NEK9 activity in mitosis is to activate NEK6 and NEK7 (Fry et al., 2017). This is thought to occur via both phosphorylation of activation loop residues and allosteric binding (Belham et al., 2003; Richards et al., 2009). Indeed, biochemical and structural studies have revealed direct interaction between residues 810-828 of NEK9 and a groove on the C-terminal lobe of the NEK7 catalytic domain (Haq et al., 2015). To determine whether the change in interphase cell morphology and migration induced by activated NEK9 is dependent on NEK6 or NEK7, cells expressing activated NEK9 were depleted of NEK6 or NEK7 (Supp. Fig. S2A). Quantitative imaging revealed that, in contrast to mock- or NEK6-depleted cells that still exhibited extended cytoplasmic protrusions upon induction of activated NEK9, depletion of NEK7 prevented formation of these protrusions (Fig. 3A and Supp. Fig. S2B). This suggested that this phenotype was dependent upon the untimely activation of NEK7 by NEK9. To confirm this hypothesis, we made use of a constitutively active mutant version of NEK7. Previous studies had revealed that, in the absence of NEK9, NEK7 adopts an auto-inhibited conformation in which the side-chain of Tyrosine-97 blocks the active site and that mutation of this residue to alanine relieves this inhibition (Richards et al., 2009).

Strikingly, transient expression of the activated NEK7-Y97A mutant, but not wild-type NEK7, caused generation of similar elongated cytoplasmic protrusions in U2OS cells (Fig. 3B, C). Consistent with the lack of effect of NEK6 depletion, expression of the equivalent activated NEK6-Y108A mutant did not cause formation of cytoplasmic protrusions but rather caused cells to become more rounded. Real-time transwell assays indicated that the increase in cell migration induced by activated NEK9 was also dependent on NEK7 but not NEK6 and, as it was detected after 10 hours, unlikely to be explained by reduced proliferation (Fig. 3D, E; and Supp. Figs. S2C, D).

To further address the role of NEK7 in this pathway, we established HeLa cell lines in which YFP tagged wild-type, catalytically-inactive (D179N) and constitutively-active (Y97A) versions of NEK7 were expressed under the control of a tetracycline inducible promoter (Supp. Fig. S3). Consistent with transient expression, inducible expression of activated NEK7 but not wild-type or kinase-inactive NEK7 resulted in the formation of microtubule rich cytoplasmic protrusions in interphase (Fig. 3F, G). Interestingly, protrusions that formed upon expression of activated NEK7 were lost upon depletion of NEK9 suggesting that NEK9 does not simply act upstream to enhance NEK7 catalytic activity (Fig. 3H). Together, these data indicate that the microtubule-dependent alteration of cell morphology and increased rate of migration that occur upon activation of NEK9 is dependent on NEK7, while similar changes induced upon activation of NEK7 require the presence of NEK9 protein.

EML4 interacts with NEK9 and promotes cell migration

To further explore the mechanism through which the NEK9-NEK7 pathway may cause this change in cell morphology and migration, myc-tagged wild-type NEK9 was immunoprecipitated from asynchronous cells and immune complexes analysed by mass spectrometry. Intriguingly, this identified not only tubulin, supporting the notion that NEK9 can interact with interphase microtubules, but also the microtubule-associated protein, EML4 (Supp. Fig. S4A-C). Previous large-scale proteomic mapping had identified EML2, EML3 and EML4 as potential binding partners of NEK6 (Ewing et al., 2007), while we have recently found that EML4 can be phosphorylated by NEK6 and NEK7 in mitosis (Adib et al., 2019

). Western blotting of immunoprecipitates prepared with antibodies against either NEK9 or EML4 confirmed interaction between endogenous EML4 and NEK9 in extracts prepared from asynchronous U2OS cells (Fig. 4A). Moreover, YFP-EML4 was found to co-precipitate as well as if not more strongly with the activated NEK9-ΔRCC1 mutant than wild-type NEK9 (Fig. 4B). As described above, NEK9 binds directly through its C-terminal region (residues 810-828) to NEK7 and NEK6, an interaction that is normally blocked in interphase by competitive interaction with the LC-8 adaptor protein (Haq et al., 2015; Regue et al., 2011). Removal of the RCC1 domain somehow relieves the auto-inhibited conformation and leads to increased

NEK9 kinase activity (Roig et al., 2002). This in turn enables autophosphorylation at Ser-944, which displaces LC-8 and allows interaction with NEK7 and NEK6 (Regue et al., 2011). Hence, we propose that activated NEK9 can potentially interact simultaneously with both EML4 and NEK7.

To investigate whether the microtubule-dependent changes in cell morphology that result from expression of activated NEK9 and NEK7 may relate to its interaction with EML4, U2OS cell lines were generated that stably expressed YFP alone or YFP-EML4. Proteins of the predicted size were expressed as determined by Western blotting, while the YFP-EML4 protein localized as expected to the microtubule network (Supp. Fig. S5A-C). In contrast to parental cells or cells expressing YFP alone, the YFP-EML4 cells exhibited a morphology similar to cells expressing activated NEK9 or NEK7 with extended cytoplasmic protrusions that were lost upon treatment with the microtubule depolymerizing agents, nocodazole or vinorelbine (Fig. 4C; and Supp. Fig. S5D). Individual cell tracking experiments as well as real-time transwell migration assays revealed that expression of YFP-EML4 also led to an increased rate, distance and velocity of migration, but reduced straightness, compared to those expressing YFP alone (Fig. 4D; and Supp. Fig. S5 E-H). To test the relationship of EML4 and NEK9 in the generation of these phenotypes, proteins were depleted in the different stable cell lines. Depletion of EML4 did not prevent the alterations in cell morphology induced upon expression of activated NEK9 (Fig. 4E; and Supp. Fig. S5I). In contrast, depletion of NEK9 or NEK7 led to loss of cytoplasmic protrusions and reduced migration in cells expressing YFP-EML4 (Fig. 4G-I; and Supp. Fig. S5J, K). Furthermore, induced expression of catalytically-inactive NEK7 prevented formation of cytoplasmic protrusions in cells overexpressing EML4 (Fig. 4I). These data indicate that overexpression of EML4 induces altered cell morphology and enhanced migration that is dependent upon NEK9 and NEK7, and can be blocked by expression of inactive NEK7.

EML4 recruits NEK9 and NEK7 to microtubules

To understand how NEK9 and NEK7 act downstream of EML4 to induce alterations in cell morphology and migration, we first examined which region of the EML4 protein may be responsible for interaction with NEK9. Co-immunoprecipitation experiments revealed that endogenous NEK9 could interact not only with full-length EML4 but also both the isolated NTD and TAPE domains (Fig. 4J). On the other hand, it did not interact with a shorter fragment of the NTD that only encompassed the trimerization motif. We then hypothesized that EML4 may promote recruitment of NEK9 to the microtubule cytoskeleton. To test this hypothesis, we examined the localization of endogenous NEK9 in cells expressing different EML4 constructs. In cells expressing the TAPE domain, endogenous NEK9 was mainly distributed in the cytoplasm with only faint detection on microtubules, whereas in cells expressing the NTD, NEK9 exhibited strong recruitment to microtubules (Fig.4K, L; and Supp.

Fig. S6A). Meanwhile, using the stable HeLa:YFP-NEK7 cell line (as localization of endogenous NEK7 is difficult to detect with current antibodies), it was found that NEK7 was recruited to microtubules upon transfection of Flag-tagged EML4 NTD, but not the TAPE domain (Fig. 4M, N; and Supp. Fig. S6B). Together, these data suggest a model in which the EML4 NTD recruits both NEK9 and NEK7 to microtubules. This explains not only how EML4 can act upstream of NEK9 and NEK7, but also why the NEK9 protein is required for activated NEK7 to promote microtubule-dependent changes in cell morphology and migration.

EML4-ALK V3 and V5, but not V1 or V2, induce altered cell morphology and migration

Considering their importance in cancer biology, we were intrigued to know whether EML4-ALK fusion proteins might also alter cell morphology and migration. To explore this possibility, we generated U2OS cell lines with stable expression of the ALK kinase domain alone or four of the different EML4-ALK variants (Fig. 5A). These included the longer variants, V1 and V2, which encode unstable proteins that do not localise to microtubules, and the shorter variants, V3 and V5, which encode stable proteins that localise to microtubules (Richards et al., 2014; Richards et al., 2015). Strikingly, microscopic analysis revealed that those cells expressing the stable variants that localise to interphase microtubules (V3 and V5) formed extended cytoplasmic protrusions, whereas those cells expressing the unstable variants that do not localise to the microtubules (V1 and V2) did not (Fig. 5B-D). Furthermore, both individual cell tracking and real-time transwell assays revealed that expression of V3 and V5 stimulated cell migration with significant increases in distance and velocity, whereas expression of V1 and V2 did not (Fig. 5E-I). Hence, expression of the short EML4-ALK variants that localize to microtubules lead to altered morphology and enhanced migration as compared to cells expressing the longer EML4-ALK variants that do not localise to microtubules.

Altered morphology and migration in EML4-ALK V3 cells depend on NEK9 and NEK7

To determine whether the changes observed in cell morphology and migration induced by EML4-ALK V3 required catalytic activity of the ALK tyrosine kinase, we first generated U2OS stable cell lines with catalytically-inactive (D1270N) versions of EML4-ALK V1 and V3. This revealed that cells expressing the inactive mutant proteins had similar length cytoplasmic protrusions as those seen in cells expressing the wild-type proteins (Fig. 6A). Second, we determined the consequences on cell migration of treatment with the ALK inhibitor, crizotinib. This did not alter the rate of migration of U2OS cells expressing EML4-ALK V3 despite preventing ALK-dependent signalling in these cells as expected (Fig. 6B, C; and Supp. Fig. S7A). Hence, we conclude that the altered morphology and enhanced migration of cells expressing EML4-ALK V3 does not require ALK activity.

As all four EML4-ALK variants under analysis here contain the EML4-NTD that can interact with NEK9, we tested whether these oncogenic fusion variants also bind NEK9. Surprisingly, co-immunoprecipitation experiments showed that endogenous NEK9 interacts with EML4-ALK V3 and V5, but not with V1 or the ALK domain alone (Fig. 6D). This reflects a similar difference in the ability of the variants to bind microtubules and, while the explanation remains unknown, it is possible that interaction with both NEK9 and microtubules is prevented in V1 and V2 either by misfolding of the NTD in the presence of the partial TAPE domain or competing association with chaperones. Real-time transwell migration assays revealed that depletion of NEK9 and NEK7 significantly reduced the migration of cells expressing EML4-ALK V3 or V5 (Fig. 6E, F; and Supp. Fig.S7B, C). Overexpression of wild-type EML4, as well as activated NEK9, can promote microtubule stabilization (Adib et al., 2019

; Houtman et al., 2007). Hence, we wished to determine whether expression of EML4-ALK V3 also caused a similar increase in microtubule stabilisation. Both Western blot analysis of acetylated tubulin expression and measurement of the rate of nocodazole-induced microtubule depolymerisation in live cells using the SiR-tubulin probe confirmed that cells expressing EML4-ALK V3 had increased microtubule stability as compared to cells expressed EML4-ALK V1 (Fig. 6G, H; and Supp. Fig. S7D).

We then expressed EML4-ALK V1 and V3 in Beas-2B bronchial epithelial cells as an alternative model for lung disease (Supp. Fig. S8A). Parental Beas-2B cells exhibit a more elongated morphology than U2OS cells and their growth is subject to contact inhibition as expected for non-cancer derived cells. For this reason, these cells were not suitable for measuring changes in cell morphology or the rate of migration in a wound-healing assay. However, they do form three-dimensional (3D) spheroids when grown in ultra-low attachment plates allowing us to analyse the consequences of expression of these fusion variants on 3D migration into Matrigel. Strikingly, we found that expression of EML4-ALK V3, but not V1, led to the generation of extended chains of Beas-2B cells typical of collective cell migration (Fig. 6I, J, K). Moreover, there was a significant reduction in the length of these chains if cells expressing EML4-ALK V3 were first depleted of NEK7 (Fig. 6L; and Supp. Fig. S8B). We therefore conclude that expression of EML4-ALK V3 but not V1 leads to NEK9 and NEK7-dependent alterations in cell morphology and migration, as well as to stabilization of microtubules.

EML4-ALK V3 NSCLC patient cells exhibit NEK9 and NEK7-dependent alteration of cell morphology and migration

To determine whether the altered cell morphology and migration observed in U2OS cell lines might contribute to tumour progression in NSCLC patients, we first examined the morphology and migration of established cell lines derived from patients expressing different EML4-ALK

variants. H3122 cells are derived from a NSCLC tumour that expresses V1, whereas H2228 are derived from a NSCLC tumour that expresses V3. Brightfield microscopy revealed that whereas H3122 cells exhibit a cobblestone appearance, H2228 cells have a spindle-like morphology with extended cytoplasmic protrusions (Fig. 7A-C). As observed in U2OS cells, the protrusions present in H2228 cells were significantly reduced in length upon depletion of either NEK7 or NEK9 (Fig. 7D, E and Supp. Fig. S8C). Real-time transwell migration assays revealed that the H2228 cells exhibited a significantly increased rate of migration as compared to H3122 cells, while this was reduced by depletion of NEK7 or NEK9 (Fig. 7F-I). Individual cell tracking experiments indicated that depletion of NEK7 or NEK9 reduced the distance and increased the straightness of migration in H2228 but not H3122 cells (Fig 7J, K; and Supp. Fig. S8D, E). Again consistent with data in U2OS cells, the elongated protrusions present in H2228 cells were not affected by treatment with the ALK inhibitor crizotinib, whereas they were reduced upon depolymerisation of microtubules with nocodazole (Fig. 7L, M). Importantly, to confirm that the differences observed in H2228 cells compared to H3122 cells were caused by the different EML4-ALK variant expressed, we first transfected H3122 cells with YFP-EML4-ALK-V3. This caused a significant increase in the length of interphase cytoplasmic protrusions in H3122 cells (Fig 7N). Second, we depleted EML4-ALK V3 from H2228 cells and found that this led to a significant reduction in cytoplasmic protrusion length (Fig. 7O, P). Together, these data provide persuasive evidence that the different behaviour of these established NSCLC patient cells results from the different EML4-ALK fusion variant that they express.

Lung cancer patients with EML-ALK V3 exhibit upregulation of NEK9

Results in established cell lines suggest that the more aggressive properties associated with EML4-ALK V3 as compared to V1 may in part be caused by a NEK9-dependent pathway that promotes cell migration. This hypothesis would require NEK9 protein to be expressed in EML4-ALK V3 tumours. To test this, we used immunohistochemistry to examine NEK9 expression in a cohort of primary tumours from patients with ALK-positive stage IV advanced lung adenocarcinoma. Remarkably, this revealed that while the majority of tumours expressing V1, V2 (or others) had low levels of NEK9 expression (64%, n=25), the majority of tumours expressing V3 or V5 had medium or high levels of NEK9 expression (91%, n=22) with an overall significant difference between the V1/V2/others and V3/V5 cohorts of $p<0.001$ (Fig. 8A, B). Intriguingly, ALK-positive lung cancer patients with medium or high NEK9 expression also exhibited worse progression-free ($p=0.027$) survival than patients with low NEK9 expression (Fig. 8C). Assessment of clinicopathological features revealed no association of NEK9 expression with gender, age or smoking history. However, EML4-ALK patients with low NEK9 expression had on average undergone more rounds of previous treatment suggestive of more prolonged and potentially less aggressive disease than those with moderate or high NEK9 expression (Supp. Tables 1 & 2). Clearly, further work will be

required to define the molecular events that underpin the apparent link between elevated NEK9, EML4-ALK variant expression and survival. However, these findings raise the exciting possibility not only that these patients could be amenable to treatments that target NEK9 or NEK7, but also that this pathway represents an important mechanism through which variants that bind microtubules accelerate lung cancer progression (Fig. 8D).

DISCUSSION

A better understanding of the processes that drive progression and metastatic dissemination of EML4-ALK tumours is urgently required as this will identify opportunities for development of new therapeutic approaches to treat ALK inhibitor-resistant NSCLC. Here, we show that the short EML4-ALK variants, including the common V3, promote microtubule-dependent changes in cell morphology and enhance cell migration in both 2D and 3D models in a manner that could promote dysplastic development and metastasis. EML4-ALK V3 is associated with poor response to ALK inhibitors suggesting additional oncogenic mechanisms that are independent of ALK tyrosine kinase activity (Woo et al., 2017). Indeed, we found that the cellular changes induced by EML4-ALK V3 were not dependent on ALK activity. Experimentally, these short variants retain the capacity to bind microtubules, in contrast to the longer variants V1 and V2 that encode destabilizing fragments of the EML4 TAPE domain and rely on the HSP90 chaperone for expression (Richards et al., 2014). We speculate that either protein misfolding or chaperone interaction blocks the ability of the longer variants to associate with and regulate microtubules. We also show that the altered cell morphology and increased migration induced by the short EML4-ALK variants are dependent on the NEK9-NEK7 kinase module. Hence, these data not only reveal a novel mechanism through which EML4-ALK variants could promote cancer progression, but also reveal new biomarkers and targets that could be exploited for the treatment of patients with these oncogenic fusions.

NEK9 is required for assembly of the microtubule-based mitotic spindle. This is consistent with the kinase achieving maximal activity in mitosis following phosphorylation by the CDK1 and PLK1 mitotic kinases (Fry et al., 2017). These phosphorylation events cause release of an auto-inhibited state that relies on the presence of an internal RCC1-like inhibitory domain (Roig et al., 2002). Upon inducible expression of an activated NEK9 mutant lacking this domain, we observed striking alterations in interphase cell morphology and enhanced cell migration. The mitotic functions of NEK9 are executed in part through phosphorylation of the microtubule nucleation adaptor protein, NEDD1/GCP-WD, and in part through activation of two other members of the NEK family, NEK6 and NEK7 (Belham et al., 2003; Kaneta and Ullrich, 2013; Roig et al., 2005; Roig et al., 2002; Sdelci et al., 2012). Interestingly, we found that depletion of NEK7, but not NEK6, prevented the altered cell morphology and enhanced migration observed in interphase cells arguing that activated NEK9 promotes these phenotypes through activation of NEK7. Indeed, similar phenotypes were generated by

expression of a constitutively active NEK7 but not NEK6 kinase. These findings are consistent with growing evidence that NEK7 has microtubule-associated functions in interphase cells, with depletion of endogenous NEK7 interfering with interphase microtubule dynamics, the centrosome duplication cycle and ciliogenesis (Cohen et al., 2013; Gupta et al., 2017; Kim et al., 2011; Kim et al., 2007; Yissachar et al., 2006). Of particular interest to our findings, a kinase-dependent role was recently described for NEK7 in stimulating dendrite growth in post-mitotic neurons. This resulted from phosphorylation by NEK7 of the kinesin motor protein Eg5, which in turn led to stabilization of microtubules (Freixo et al., 2018). As EML4 is highly expressed in neurons, we speculate that modulation of microtubule organization leading to altered neuronal morphology and migration may represent the normal physiological role for the EML4-NEK9-NEK7 pathway identified here. However, NEK7 can phosphorylate other motor proteins to control microtubule organization and interact with additional regulators of the microtubule and actin networks, offering alternative mechanisms through which this pathway could operate (Cullati et al., 2017; de Souza et al., 2014).

The discovery of EML4 as a binding partner for NEK9 provides new insight into how NEK9 might regulate microtubule dynamics. The EMLs are a family of relatively poorly characterized MAPs (Fry et al., 2016). Humans have six EMLs of which EML1, 2, 3 and 4 share a similar organization consisting of an NTD that encompasses a trimerization motif and basic region that binds microtubules, and a C-terminal TAPE domain that binds tubulin heterodimers (Richards et al., 2014; Richards et al., 2015). The possibility that EMLs may be interacting partners of NEKs was first raised by a proteomic study that identified association of NEK6 not only with NEK7 and NEK9, but also EML2, EML3 and EML4 (Ewing et al., 2007). We identified EML4, as well as tubulin, in a mass spectrometry analysis for NEK9 binding partners, while interaction of endogenous EML4 and NEK9 was confirmed by Western blotting. Co-immunoprecipitation studies revealed that NEK9 can bind to the isolated NTD of EML4, as well as to the EML4-ALK V3 and V5 proteins. Interestingly, it did not bind to EML4-ALK V1 despite this variant encoding the complete NTD. This suggests that misfolding or binding of chaperones might prevent interaction with NEK9 as well as microtubules. Further studies revealed that the EML4 NTD was capable of recruiting both NEK9 and NEK7 to microtubules. This suggests that binding of the EML4 NTD to microtubules and NEK9 are not mutually exclusive, although the fact that NEK9 and the EML4 NTD form dimers and trimers, respectively, means that this recruitment could rely on oligomerization of these proteins. We propose that recruitment of NEK7 relies on its direct interaction with NEK9, although do not rule out an independent interaction with EML4. However, the fact that NEK9 is required for these morphological consequences even in the presence of activated NEK7 suggest that NEK9 plays an essential role potentially in targeting NEK7 to its downstream substrates. Moreover, although we have shown that expression of activated NEK9 and EML4-ALK V3 leads to stabilization of microtubules, further work is required to establish the mechanisms through which this pathway regulates cell morphology and migration.

Of major clinical significance is the fact that EML4-ALK fusion proteins act as oncogenic drivers in ~5% of NSCLC patients (Soda et al., 2007). Unscheduled activation of the ALK tyrosine kinase is primarily responsible for driving tumorigenesis as demonstrated by the fact that ALK inhibitors block transformation. First and second generation ALK inhibitors have revolutionized survival outcomes in ALK-positive lung cancer patients; however resistance is inevitable emerging through point mutations in the catalytic domain as well as through bypass pathways (Liao et al., 2015; Rolfo et al., 2014). Alternative targeted therapies would therefore be highly attractive and, in the case of the longer variants, HSP90 inhibitors could provide an option. The longer variants are unstable proteins as a result of expressing an incomplete fragment of the highly structured TAPE domain. In the absence of the HSP90 chaperone they are rapidly degraded by the proteasome leading to loss of downstream proliferative signalling (Richards et al., 2014). HSP90 inhibitors have been tested in ALK-positive patients although to date clinical trials have yet to prove their efficacy (Katayama et al., 2015; Workman and van Montfort, 2014). The short variants though are not dependent on HSP90 for their expression and HSP90 inhibitor treatment is unlikely to be effective. Moreover, EML4-ALK V3 tumours appear less sensitive to ALK inhibitors in the first place emphasizing the need for alternative treatments for these particular patients (Woo et al., 2017). Demonstration that the downstream consequences on cell morphology and migration induced by these short variants is dependent on NEK9 and NEK7, but not ALK activity, raises the tantalizing prospect that inhibitors of this pathway may be beneficial in EML4-ALK V3 cancers where metastasis and ALK inhibitor resistance underpin lethality (Christopoulos et al., 2018). Although we have no evidence that inhibiting this pathway promotes cytotoxicity, the ability to block migration and invasion with so-called ‘migrastatics’ offers huge potential benefits in slowing disease progression in patients with solid cancers (Gandalovicova et al., 2017).

The significant correlation in patient samples between elevated NEK9 expression and EML4-ALK V3 is particularly intriguing as it implicates this pathway in the high metastatic potential of these tumours (Christopoulos et al., 2018; Doebele et al., 2012). However, although the association of elevated NEK9 with V3 and V5 was significant, expression does not necessarily reflect activation and it will be important in the future to assess the catalytic activity of NEK9 and NEK7 in these tumours. Moreover, we cannot rule out that tumour cells with this variant exert positive selection for high expression of NEK9 either due to its role as a downstream target or as a result of their increased aggressiveness. Nevertheless, the reduced progression-free survival of patients with increased NEK9 expression potentially explains the poor response of these patients to ALK-based therapies, despite the fact that the different EML4-ALK variants bind ALK inhibitors with similar affinity (Heuckmann et al., 2012). This also adds further evidence that NEK9 may be an important prognostic factor for EML4-

ALK lung cancers and supports the hypothesis that targeting NEK9 or NEK7 could be beneficial in patients with EML4-ALK V3.

Finally, it is interesting to note that EML proteins are involved in other oncogenic fusions, including the EML1-ABL1 fusion found in T-cell acute lymphoblastic leukaemia (ALL) (De Keersmaecker et al., 2005). Whether these also localise to microtubules and alter cell morphology and migration in a manner that is dependent on the microtubule network and the NEK9-NEK7 kinase module will be important to examine. Standard treatments for many cancers, including NSCLC and ALL, often involve microtubule poisons, such as vinorelbine or paclitaxel. Hence, it will also be worthwhile to explore the possibility that EML4-ALK variant status affects response to these drugs, and test whether there could be patient benefit in combining microtubule poisons with targeted agents against ALK, HSP90 or indeed NEK9 or NEK7.

MATERIALS & METHODS

Plasmid construction and mutagenesis

Full-length EML4 cDNA was isolated by PCR from human cDNA (Clontech) and subcloned into a version of pcDNA3 or pcDNA3.1-hygro (Invitrogen) providing N-terminal YFP- or Flag-tags. YFP-tagged EML4-ALK variants and fragments of EML4, and Flag-tagged NEK6 and NEK7 constructs were generated as previously described(O'Regan and Fry, 2009; Richards et al., 2014; Richards et al., 2015). A full-length Myc tagged cDNA expressing human NEK9 (NM_001329237.1) was subcloned into the pVLX-Tight-Puro vector (Clontech). The RCC1 domain was deleted using the Quickchange® II XL Site-Directed Mutagenesis Kit according to manufacturer's instructions (Stratagene) using the primer sequences, 5'-gctgtagtaacatcacgaaccagtatccgttccaatagcagtggcttatcc and 5'-ggataagccactgctattggaacggatactggttcgtgatgttactacagc. Point mutations in the NEK7, NEK6 and ALK catalytic domains were also introduced using the Quickchange® II XL Site-Directed Mutagenesis Kit. Constructs were confirmed by DNA sequencing (University of Leicester).

Cell culture, drug treatments and transfection

HeLa, U2OS and derived stable cell lines were grown in Dulbecco's modified Eagle's medium (DMEM) with GlutaMAX™-I (Invitrogen) supplemented with 10% heat-inactivated fetal bovine serum (HI-FBS), 100 U/ml penicillin, and 100 µg/ml streptomycin, at 37˚C in a 5% CO_2 atmosphere. H3122 and H2228 cells were grown in RPMI 1640 medium (Invitrogen) supplemented with 10% HI-FBS, 100 U/ml penicillin and 100 µg/ml streptomycin. All cell lines were obtained from ATCC within the last 10 years, stored in liquid nitrogen and maintained in culture for a maximum of 2 months. We relied on the provenance of the original collections

for authenticity, while mycoplasma infection was avoided through bimonthly tests using an in-house PCR-based assay. Doxycycline-inducible NEK9 stable U2OS cell lines were generated through lentiviral transduction of parental U2OS cells stably carrying the pVLX-Tet-On-Advance vector (Clontech, PT3990-5). Briefly, NEK9 lentiviral particles for each construct were harvested from transfected 293T packaging cells using the Lenti-X™ HTX Packaging System (Clontech), transduced into U2OS parental cells and selected in fresh media supplemented with 2 mg/ml of G418 and 1 µg/ml puromycin over several days. To maintain expression of constructs, culture media was supplemented with 1 ug/ml of G418 and 800 ng/ml of puromycin. For induction of constructs, doxycycline was added to growth media at a final concentration of 1 µg/ml for 72 h, unless otherwise stated. Doxycycline-inducible HeLa:YFP-NEK7 cell lines were generated via co-transfection of parental HeLa cells which stably express the lacZ-Zeocin™ fusion gene and Tet repressor from pFRT/lacZeo and pcDNA6/TR plasmids, respectively, with the appropriate pcDNA5/FRT/TO-YFP-NEK7 vector and the Flp recombinase expression vector, pOG44. After 48 h cells were incubated in selective media containing 200 µg/ml hygromycin B and resistant clones selected and expanded. To maintain expression in stable cell lines, media was supplemented with 200 µm/ml hygromycin B (Invitrogen). For induction of NEK7 constructs, doxycycline was added at a final concentration of 1 µg/ml for 72 h unless otherwise stated. Constitutively expressing EML4 and EML4-ALK cell lines were generated by transfecting the relevant construct into U2OS cells. After 48 h cells were incubated in selective media containing 100 µg/ml hygromycin B (Invitrogen). To maintain expression in stable cell lines, media was supplemented with 100 µg/ml hygromycin. Where indicated, cells were treated with 200 ng/ml nocodazole (Sigma), 20 nM vinorelbine (Sigma) or 100 nM Crizotinib (Selleck). Transient transfections were performed with Lipofectamine 2000 (Invitrogen) according to manufacturer's instructions. For flow cytometry, cells were fixed in ice-cold 70% ethanol before DNA was labelled with 5 µg/ml propidium iodide. Analysis was performed using a FACSCanto II instrument and FACSDiva software (BD Biosciences).

Preparation of cell extracts, SDS-PAGE and Western blotting

Cells were lysed in RIPA lysis buffer (50 mM Tris-HCl pH 8, 150 mM NaCl, 1% v/v Nonidet P-40, 0.1% w/v SDS, 0.5% w/v sodium deoxycholate, 5 mM NaF, 5 mM β-glycerophosphate, 30 µg/ml RNase, 30 µg/ml DNase I, 1x Protease Inhibitor Cocktail, 1 mM PMSF) prior to analysis by SDS-PAGE and Western blotting. Primary antibodies were GFP (0.2 µg/ml, cat# ab6556, Abcam), α-tubulin (0.1 µg/ml, clone B512,cat# T5168, Sigma), myc (1:1000, clone 9B11 cat# 2276, Cell Signalling Technologies), NEK9 (0.8 µg/ml, cat# sc-50765, Santa Cruz Biotechnology), EML4 (0.2 µg/ml, cat# A310-908A, Bethyl Laboratories), Flag (0.5 µm/ml, clone M2, cat# F3165, Sigma), acetylated tubulin (0.5 µg/ml, clone 6-11 B-1 cat# T6793, , Sigma) ALK (1:2000, cat# 3633, Cell Signaling technology), pALK (1:1000, cat# 3341, Cell Signaling Technology) and GAPDH (1 µg/ml, cat# 2118, Cell Signalling Technology).

Secondary antibodies used were anti-rabbit, anti-mouse or anti-goat horseradish peroxidase (HRP)-labelled IgGs (1:1000; cat# A6154, A4416 and A5420, respectively, Sigma). Western blots were detected using enhanced chemiluminescence (Pierce).

RNAi

Cells at 30–40% confluency were cultured in Opti-MEM Reduced Serum Medium and transfected with 50 nM siRNA duplexes using Oligofectamine (Invitrogen) according to the manufacturer's instructions. 72 hours after transfection, cells were either fixed for immunocytochemistry or prepared for Western blot. siRNA oligos were directed against NEK9, AM51334-1113 and -1115 silencer select duplexes (Ambion) or EML4, HSS120688 and Hss178451 On-Target Plus duplexes (Dharmacon); siRNA duplexes for NEK6 and NEK7 were as previously described (O'Regan and Fry, 2009)[20].

Immunoprecipitation, kinase assay and mass spectrometry

Cells were harvested by incubation with 1x PBS+0.5 mM EDTA and pelleted by centrifugation prior to being lysed in NEB lysis buffer(Fry and Nigg, 1997). Lysates were immunoprecipitated using antibodies against NEK9 (0.8 µg/ml, cat# sc-50765, Santa Cruz Biotechnologies), EML4 (0.4 µg/ml, cat# A310-908A, Bethyl Laboratories), myc (1:1000, clone 9B11 cat# 2276, Cell Signaling Technologies) or GFP (0.2 µg/ml, cat# ab6556, Abcam). Proteins that co-precipitated with myc-NEK9 were excised from gels and subjected to in-gel tryptic digestion prior to LC-MS/MS using an RSLCnano HPLC system (Dionex, UK) and an LTQ-Orbitrap-Velos mass spectrometer (Thermo Scientific). The raw data file obtained from each LC-MS/MS acquisition was processed using Proteome Discoverer (version 1.4, Thermo Scientific), searching each file in turn using Mascot (version 2.2.04, Matrix Science Ltd.) against the human reference proteome downloaded from UniProtKB (Proteome ID: UP000005640). The peptide tolerance was set to 5 ppm and the MS/MS tolerance set to 0.6 Da. The output from Proteome Discoverer was further processed using Scaffold Q+S (version 4.0.5, Proteome Software). Upon import, the data was searched using X!Tandem (The Global Proteome Machine Organization). PeptideProphet and ProteinProphet (Institute for Systems Biology) probability thresholds of 95% were calculated from the decoy searches and Scaffold used to calculate an improved 95% peptide and protein probability threshold based on the two search algorithms.

Fixed and time-lapse microscopy

Cells grown on acid-etched coverslips were fixed and permeabilised by incubation in ice-cold methanol at -20˚C for a minimum of 20 min. Cells were blocked with PBS supplemented with 3% BSA and 0.2% Triton X-100 prior to incubation with the appropriate primary antibody diluted in PBS supplemented with 3% BSA and 0.2% Triton X-100. Primary antibodies used were against GFP (0.5 µg/ml, cat# ab6556; Abcam); α-tubulin (0.1 µg/ml, clone B512,cat# T5168, Sigma), myc (1:1000, clone 9B11 cat# 2276, Cell Signalling Technologies), Flag (0.5 µg/ml, clone M2, cat# F3165, Sigma-Aldrich), NEK9 (0.8 µg/ml, cat# sc-50765, Santa Cruz Biotechnology), γ-tubulin (0.2 µg/ml, cat# T3559, Sigma). Secondary antibodies were Alexa Fluor 488, 594 and 647 donkey anti-rabbit, donkey anti-mouse and donkey anti-goat IgGs (1 µg/ml; cat# A32790, A32744 and AS32849, respectively, Invitrogen). DNA was stained with 0.8 µg/ml Hoechst 33258. For actin visualisation, cells were fixed using 3.7% formaldehyde and stained using phalloidin-TRITC (1:200). Imaging was performed on a Leica TCS SP5 confocal microscope equipped with an inverted microscope (DMI6000 B; Leica) using a 63x oil objective (numerical aperture, 1.4). Z stacks comprising 30–50 0.3-µm sections were acquired using LAS-AF software (Leica), and deconvolution of 3D image stacks performed using Huygens software (Scientific Volume Imaging). For super-resolution radial fluctuations (SRRF) microscopy a VisiTech infinity 3 confocal microscope fitted with Hamamatsu C11440 -22CU Flash 4.0 V2 sCMOS camera and a Plan Apo 100 x objective (NA 1.47) was used. 100 images from the same slice were captured per channel and processed using the nanoJ-SRRF plugin in Fiji. Immunohistochemistry with NEK9 antibodies (Abcam, ab138488; 1:500) was performed on NSCLC patients with EML4-ALK fusions.

Phase contrast and time-lapse microscopy was carried out using a Nikon eclipse Ti inverted microscope using a Plan Fluor 10x DIC objective (NA 0.3) or a Plan Fluor 40x objective (NA 1.3). Images were captured using an Andor iXonEM+ EMCCD DU 885 camera and NIS elements software (Nikon). For time-lapse imaging, cells were cultured in 6-well dishes and maintained on the stage at 37°C in an atmosphere supplemented with 5% CO_2 using a microscope temperature control system (Life Imaging Services) with images acquired every 15 min for ≥24 h. Videos were prepared using ImageJ (National Institutes of Health). Cell protrusions were measured using Fiji. The length of protrusion was defined as the distance from the edge of the nucleus of the cell to the furthest point of the plasma membrane. For each experiment 50 cells were measured per condition.

Individual Cell Tracking Assays

To allow automated detection of individual cells for tracking analysis cells were transfected with YFP alone and subjected to time lapse imaging as appropriate. Individual cell tracking was then analysed using Imaris (Bitplane). Fluorescent cells were identified using the Imaris

spots function and subsequently the Imaris TrackLineage algorithm was used to identify movements or tracks of these cells through the entire time period and thus provide numerical values for parameters such as speed and distance. For each experiment 25 tracks were measured per condition.

Live-cell microtubule stability assays

For live cell microtubule stability assays cells were grown in µ-well 8 well chamber slides (ibidi). Cells were incubated with 25 nM SiR-Tubulin (Cytoskeleton Inc.) for 4 h prior to imaging, 10 images were captured prior to addition of nocodazole and the drug was then added and a further 15 images were captured. Z stacks comprising of approximately 10 0.5 µm sections were captured every 30 s for 7 mins. Images were cropped to single cells and deconvolved prior to analysis in Matlab. For each experiment 10 cells were measured per treatment.

Cell migration assays

For scratch-wound assays, cells were grown to 95% confluency in 6 well dishes before a pipette tip was used to scrape a 0.5 - 1 µm line across the width of the well. Cells were washed 3-5 x in pre-warmed media and either imaged by time-lapse microscopy or incubated at 37^{o}C for 6 h before being processed for immunofluorescence microscopy. Cell migration in real time was analysed using the xCELLigence Real-Time Cell Analyzer (RTCA) DC equipment (AECA Biosciences) and CIM-16 plates, a 16 well system where each well is composed of upper and lower chambers separated by an 8 µm microporous membrane. Cells were grown in serum free medium for 24 h before being seeded in serum free medium into the upper chamber; complete medium containing 10% FBS was used as a chemo-attractant in the lower chamber of the plate and migration determined as the relative impedance change (cell migration index) across microelectronic sensors integrated into the membrane, where cell migration index = (impedance at timepoint n/impedance in the absence of cells)/nominal impedance value. Measurements were taken every 15 mins for 48 h.

3D Spheroid Invasion Assays

Spheroids were grown in ultra-low attachment 96-well plates (Corning) for 24hr hours, before EML4-ALK expression was induced using 1ug/ml doxycycline and siRNA applied for a further 72hr. On day 5, Matrigel (Corning) was added to wells at 2.5mg/ml and further induction and siRNA treatment applied. Spheroids were imaged at 0hr and 72hr after addition of Matrigel using a VisiTech infinity 3 confocal microscope fitted with Hamamatsu C11440 -22CU Flash 4.0 V2 sCMOS camera and 10x/0.3 Pan Fluor DIC L/N objective. Resulting images were analysed using Fiji software. 10 invasive strands were measured per cell and 6 spheriods were measured per condition.

Statistical analysis

All quantitative data represent means ± SD of three independent experiments. Statistical analyses on data shown in histograms were performed using a one-tailed unpaired Student's *t* test assuming unequal variance or a one-way analysis of variance followed by post hoc testing for analysis of 2 data sets and multiple data sets, respectively. For RTCA cell migration data and microtubule stability assays, which generated line plots, the area under the curve was calculated for each data set and statistical analysis was performed on these data using either a one-tailed unpaired Students t-test assuming unequal variance (2 data sets) or a one way ANOVA (more than 2 data sets). For patient data, statistical significance was calculated using χ^2 test. *p*-values represent *, $p< 0.05$; **, $p< 0.01$; ***, $p< 0.001$. n.s., non-significant.

Statement of ethics

All work involving patient samples was approved by the Institutional Review Board of Asan Medical Center. All data was subject to an anonymizing program to retrieve patient lists which removes patient hospital ID and assigns a new research ID to each patient.

Data availability statement

The data that support the findings of this study are available from the corresponding author upon reasonable request.

ACKNOWLEDGMENTS

We are very grateful to Patrick Meraldi and his colleagues (University of Geneva) for introducing us to the kinetic SiR-tubulin microtubule depolymerization assay. We acknowledge the University of Leicester Core Biotechnology Services for support with cloning, mass spectrometry, DNA sequencing and microscopy. This work was supported by grants to A.M.F. from Worldwide Cancer Research (13-0042 and 16-0119), the Wellcome Trust (082828 and 097828) and Cancer Research UK (C1362/A180081); to R.B. from Cancer Research UK (C24461/A23302); to R.B. and J.C. from MRC-KHIDI (MC_PC_17103) U.K. and MRC-KHIDI (HI17C1975) Republic of Korea; to S.J.C. from Cancer Research UK (Senior Cancer Research Fellowship A12102); and to G.B. from Weston Park Hospital Cancer Charity (Large Project Grant CA164).

AUTHOR CONTRIBUTIONS

L.O'R., G.B, R.A., C.G.W., H.J.J. and E.L.R. undertook the experiments and provided comments on the manuscript. M.R. designed and generated the YFP-EML4 and YFP-EML4-ALK constructs; P.A.J.M., S.J.C., D.A.F., J.C. and R.B. contributed to study design and provided comments on the manuscript. L.O'R. and A.M.F. designed and supervised the project and wrote the manuscript.

REFERENCES

Adib, R., Montgomery, J. M., Atherton, J., O'Regan, L., Richards, M. W., Straatman, K. R., Roth, D., Straube, A., Bayliss, R., Moores, C. A. et al. (2019). Mitotic phosphorylation by NEK6 and NEK7 reduces the microtubule affinity of EML4 to promote chromosome congression. *Sci Signal* **12**, 594.

Bayliss, R., Choi, J., Fennell, D. A., Fry, A. M. and Richards, M. W. (2016). Molecular mechanisms that underpin EML4-ALK driven cancers and their response to targeted drugs. *Cell Mol Life Sci* **73**, 1209-24.

Belham, C., Roig, J., Caldwell, J. A., Aoyama, Y., Kemp, B. E., Comb, M. and Avruch, J. (2003). A mitotic cascade of NIMA family kinases. Nercc1/Nek9 activates the Nek6 and Nek7 kinases. *J Biol Chem* **278**, 34897-909.

Chatterjee, S., Bhattacharya, S., Socinski, M. A. and Burns, T. F. (2016). HSP90 inhibitors in lung cancer: promise still unfulfilled. *Clin Adv Hematol Oncol* **14**, 346-56.

Chen, Z., Sasaki, T., Tan, X., Carretero, J., Shimamura, T., Li, D., Xu, C., Wang, Y., Adelmant, G. O., Capelletti, M. et al. (2010). Inhibition of ALK, PI3K/MEK, and HSP90 in murine lung adenocarcinoma induced by EML4-ALK fusion oncogene. *Cancer Res* **70**, 9827-36.

Choi, Y. L., Soda, M., Yamashita, Y., Ueno, T., Takashima, J., Nakajima, T., Yatabe, Y., Takeuchi, K., Hamada, T., Haruta, H. et al. (2010). EML4-ALK mutations in lung cancer that confer resistance to ALK inhibitors. *N Engl J Med* **363**, 1734-9.

Choi, Y. L., Takeuchi, K., Soda, M., Inamura, K., Togashi, Y., Hatano, S., Enomoto, M., Hamada, T., Haruta, H., Watanabe, H. et al. (2008). Identification of novel isoforms of the EML4-ALK transforming gene in non-small cell lung cancer. *Cancer Res* **68**, 4971-6.

Christopoulos, P., Endris, V., Bozorgmehr, F., Elsayed, M., Kirchner, M., Ristau, J., Buchhalter, I., Penzel, R., Herth, F. J., Heussel, C. P. et al. (2018). EML4-ALK fusion variant V3 is a high-risk feature conferring accelerated metastatic spread, early treatment failure and worse overall survival in ALK(+) non-small cell lung cancer. *Int J Cancer* **142**, 2589-2598.

Cohen, S., Aizer, A., Shav-Tal, Y., Yanai, A. and Motro, B. (2013). Nek7 kinase accelerates microtubule dynamic instability. *Biochim Biophys Acta* **1833**, 1104-13.

Crystal, A. S., Shaw, A. T., Sequist, L. V., Friboulet, L., Niederst, M. J., Lockerman, E. L., Frias, R. L., Gainor, J. F., Amzallag, A., Greninger, P. et al. (2014). Patient-derived models of acquired resistance can identify effective drug combinations for cancer. *Science* **346**, 1480-6.

Cullati, S. N., Kabeche, L., Kettenbach, A. N. and Gerber, S. A. (2017). A bifurcated signaling cascade of NIMA-related kinases controls distinct kinesins in anaphase. *J Cell Biol* **216**, 2339-2354.

De Keersmaecker, K., Graux, C., Odero, M. D., Mentens, N., Somers, R., Maertens, J., Wlodarska, I., Vandenberghe, P., Hagemeijer, A., Marynen, P. et al. (2005). Fusion of EML1 to ABL1 in T-cell acute lymphoblastic leukemia with cryptic t(9;14)(q34;q32). *Blood* **105**, 4849-52.

de Souza, E. E., Meirelles, G. V., Godoy, B. B., Perez, A. M., Smetana, J. H., Doxsey, S. J., McComb, M. E., Costello, C. E., Whelan, S. A. and Kobarg, J. (2014). Characterization of the human Nek7 interactome suggests catalytic and regulatory properties distinct from Nek6. *J Proteome Res* **13**, 4074-4090.

Doebele, R. C., Lu, X., Sumey, C., Maxson, D. A., Weickhardt, A. J., Oton, A. B., Bunn, P. A., Jr., Baron, A. E., Franklin, W. A., Aisner, D. L. et al. (2012). Oncogene status predicts patterns of metastatic spread in treatment-naive nonsmall cell lung cancer. *Cancer* **118**, 4502-11.

Ewing, R. M., Chu, P., Elisma, F., Li, H., Taylor, P., Climie, S., McBroom-Cerajewski, L., Robinson, M. D., O'Connor, L., Li, M. et al. (2007). Large-scale mapping of human protein-protein interactions by mass spectrometry. *Mol Syst Biol* **3**, 89.

Freixo, F., Martinez Delgado, P., Manso, Y., Sanchez-Huertas, C., Lacasa, C., Soriano, E., Roig, J. and Luders, J. (2018). NEK7 regulates dendrite morphogenesis in neurons via Eg5-dependent microtubule stabilization. *Nat Commun* **9**, 2330.

Fry, A. M., Bayliss, R. and Roig, J. (2017). Mitotic Regulation by NEK Kinase Networks. *Front Cell Dev Biol* **5**, 102.

Fry, A. M. and Nigg, E. A. (1997). Characterization of mammalian NIMA-related kinases. *Methods Enzymol* **283**, 270-82.

Fry, A. M., O'Regan, L., Montgomery, J., Adib, R. and Bayliss, R. (2016). EML proteins in microtubule regulation and human disease. *Biochem Soc Trans* **44**, 1281-1288.

Fry, A. M., O'Regan, L., Sabir, S. R. and Bayliss, R. (2012). Cell cycle regulation by the NEK family of protein kinases. *J. Cell Sci.* **125**, 4423-4433.

Gandalovicova, A., Rosel, D., Fernandes, M., Vesely, P., Heneberg, P., Cermak, V., Petruzelka, L., Kumar, S., Sanz-Moreno, V. and Brabek, J. (2017). Migrastatics-Anti-metastatic and Anti-invasion Drugs: Promises and Challenges. *Trends Cancer* **3**, 391-406.

Gupta, A., Tsuchiya, Y., Ohta, M., Shiratsuchi, G. and Kitagawa, D. (2017). NEK7 is required for G1 progression and procentriole formation. *Mol Biol Cell* **28**, 2123-2134.

Haq, T., Richards, M. W., Burgess, S. G., Gallego, P., Yeoh, S., O'Regan, L., Reverter, D., Roig, J., Fry, A. M. and Bayliss, R. (2015). Mechanistic basis of Nek7 activation through Nek9 binding and induced dimerization. *Nat Commun* **6**, 8771.

Heuckmann, J. M., Balke-Want, H., Malchers, F., Peifer, M., Sos, M. L., Koker, M., Meder, L., Lovly, C. M., Heukamp, L. C., Pao, W. et al. (2012). Differential protein stability and ALK inhibitor sensitivity of EML4-ALK fusion variants. *Clin Cancer Res* **18**, 4682-90.

Houtman, S. H., Rutteman, M., De Zeeuw, C. I. and French, P. J. (2007). Echinoderm microtubule-associated protein like protein 4, a member of the echinoderm microtubule-associated protein family, stabilizes microtubules. *Neuroscience* **144**, 1373-82.

Hrustanovic, G., Olivas, V., Pazarentzos, E., Tulpule, A., Asthana, S., Blakely, C. M., Okimoto, R. A., Lin, L., Neel, D. S., Sabnis, A. et al. (2015). RAS-MAPK dependence underlies a rational polytherapy strategy in EML4-ALK-positive lung cancer. *Nat Med* **21**, 1038-47.

Kaneta, Y. and Ullrich, A. (2013). NEK9 depletion induces catastrophic mitosis by impairment of mitotic checkpoint control and spindle dynamics. *Biochem Biophys Res Commun* **442**, 139-46.

Katayama, R., Lovly, C. M. and Shaw, A. T. (2015). Therapeutic targeting of anaplastic lymphoma kinase in lung cancer: a paradigm for precision cancer medicine. *Clin Cancer Res* **21**, 2227-35.

Kim, S., Kim, S. and Rhee, K. (2011). NEK7 is essential for centriole duplication and centrosomal accumulation of pericentriolar material proteins in interphase cells. *J Cell Sci* **124**, 3760-70.

Kim, S., Lee, K. and Rhee, K. (2007). NEK7 is a centrosomal kinase critical for microtubule nucleation. *Biochem Biophys Res Commun* **360**, 56-62.

Kwak, E. L., Bang, Y. J., Camidge, D. R., Shaw, A. T., Solomon, B., Maki, R. G., Ou, S. H., Dezube, B. J., Janne, P. A., Costa, D. B. et al. (2010). Anaplastic lymphoma kinase inhibition in non-small-cell lung cancer. *N Engl J Med* **363**, 1693-703.

Li, Q. and Suprenant, K. A. (1994). Molecular characterization of the 77-kDa echinoderm microtubule-associated protein. Homology to the beta-transducin family. *J Biol Chem* **269**, 31777-84.

Liao, B. C., Lin, C. C., Shih, J. Y. and Yang, J. C. (2015). Treating patients with ALK-positive non-small cell lung cancer: latest evidence and management strategy. *Ther Adv Med Oncol* **7**, 274-90.

Lin, E., Li, L., Guan, Y., Soriano, R., Rivers, C. S., Mohan, S., Pandita, A., Tang, J. and Modrusan, Z. (2009). Exon array profiling detects EML4-ALK fusion in breast, colorectal, and non-small cell lung cancers. *Mol Cancer Res* **7**, 1466-76.

Lukinavicius, G., Reymond, L., D'Este, E., Masharina, A., Gottfert, F., Ta, H., Guther, A., Fournier, M., Rizzo, S., Waldmann, H. et al. (2014). Fluorogenic probes for live-cell imaging of the cytoskeleton. *Nat Methods* **11**, 731-3.

McCoach, C. E., Le, A. T., Gowan, K., Jones, K., Schubert, L., Doak, A., Estrada-Bernal, A., Davies, K. D., Merrick, D. T., Bunn, P. A., Jr. et al. (2018). Resistance Mechanisms to Targeted Therapies in ROS1(+) and ALK(+) Non-small Cell Lung Cancer. *Clin Cancer Res* **24**, 3334-3347.

Moniz, L., Dutt, P., Haider, N. and Stambolic, V. (2011). Nek family of kinases in cell cycle, checkpoint control and cancer. *Cell Div* **6**, 18.

O'Regan, L. and Fry, A. M. (2009). The Nek6 and Nek7 protein kinases are required for robust mitotic spindle formation and cytokinesis. *Mol Cell Biol* **29**, 3975-90.

Regue, L., Sdelci, S., Bertran, M. T., Caelles, C., Reverter, D. and Roig, J. (2011). DYNLL/LC8 protein controls signal transduction through the Nek9/Nek6 signaling module by regulating Nek6 binding to Nek9. *J Biol Chem* **286**, 18118-29.

Richards, M. W., Law, E. W., Rennalls, L. P., Busacca, S., O'Regan, L., Fry, A. M., Fennell, D. A. and Bayliss, R. (2014). Crystal structure of EML1 reveals the basis for Hsp90 dependence of oncogenic EML4-ALK by disruption of an atypical beta-propeller domain. *Proc Natl Acad Sci U S A* **111**, 5195-200.

Richards, M. W., O'Regan, L., Mas-Droux, C., Blot, J. M., Cheung, J., Hoelder, S., Fry, A. M. and Bayliss, R. (2009). An autoinhibitory tyrosine motif in the cell-cycle-regulated Nek7 kinase is released through binding of Nek9. *Mol Cell* **36**, 560-70.

Richards, M. W., O'Regan, L., Roth, D., Montgomery, J. M., Straube, A., Fry, A. M. and Bayliss, R. (2015). Microtubule association of EML proteins and the EML4-ALK variant 3 oncoprotein require an N-terminal trimerization domain. *Biochem J* **467**, 529-36.

Rikova, K., Guo, A., Zeng, Q., Possemato, A., Yu, J., Haack, H., Nardone, J., Lee, K., Reeves, C., Li, Y. et al. (2007). Global survey of phosphotyrosine signaling identifies oncogenic kinases in lung cancer. *Cell* **131**, 1190-203.

Roig, J., Groen, A., Caldwell, J. and Avruch, J. (2005). Active Nercc1 protein kinase concentrates at centrosomes early in mitosis and is necessary for proper spindle assembly. *Mol Biol Cell* **16**, 4827-40.

Roig, J., Mikhailov, A., Belham, C. and Avruch, J. (2002). Nercc1, a mammalian NIMA-family kinase, binds the Ran GTPase and regulates mitotic progression. *Genes Dev* **16**, 1640-58.

Rolfo, C., Passiglia, F., Castiglia, M., Raez, L. E., Germonpre, P., Gil-Bazo, I., Zwaenepoel, K., De Wilde, A., Bronte, G., Russo, A. et al. (2014). ALK and crizotinib: after the honeymoon...what else? Resistance mechanisms and new therapies to overcome it. *Transl Lung Cancer Res* **3**, 250-61.

Sasaki, T., Rodig, S. J., Chirieac, L. R. and Janne, P. A. (2010). The biology and treatment of EML4-ALK non-small cell lung cancer. *Eur J Cancer* **46**, 1773-80.

Sdelci, S., Bertran, M. T. and Roig, J. (2011). Nek9, Nek6, Nek7 and the separation of centrosomes. *Cell Cycle* **10**, 3816-7.

Sdelci, S., Schutz, M., Pinyol, R., Bertran, M. T., Regue, L., Caelles, C., Vernos, I. and Roig, J. (2012). Nek9 phosphorylation of NEDD1/GCP-WD contributes to Plk1 control of gamma-tubulin recruitment to the mitotic centrosome. *Curr Biol* **22**, 1516-23.

Shaw, A. T., Kim, D. W., Nakagawa, K., Seto, T., Crino, L., Ahn, M. J., De Pas, T., Besse, B., Solomon, B. J., Blackhall, F. et al. (2013). Crizotinib versus chemotherapy in advanced ALK-positive lung cancer. *N Engl J Med* **368**, 2385-94.

Soda, M., Choi, Y. L., Enomoto, M., Takada, S., Yamashita, Y., Ishikawa, S., Fujiwara, S., Watanabe, H., Kurashina, K., Hatanaka, H. et al. (2007). Identification of the transforming EML4-ALK fusion gene in non-small-cell lung cancer. *Nature* **448**, 561-6.

Suprenant, K. A., Dean, K., McKee, J. and Hake, S. (1993). EMAP, an echinoderm microtubule-associated protein found in microtubule-ribosome complexes. *J Cell Sci* **104**, 445-50.

Vaz Meirelles, G., Ferreira Lanza, D. C., da Silva, J. C., Santana Bernachi, J., Paes Leme, A. F. and Kobarg, J. (2010). Characterization of hNek6 interactome reveals an important role for its short N-terminal domain and colocalization with proteins at the centrosome. *J Proteome Res* **9**, 6298-316.

Woo, C. G., Seo, S., Kim, S. W., Jang, S. J., Park, K. S., Song, J. Y., Lee, B., Richards, M. W., Bayliss, R., Lee, D. H. et al. (2017). Differential protein stability and clinical responses of EML4-ALK fusion variants to various ALK inhibitors in advanced ALK-rearranged non-small cell lung cancer. *Ann Oncol* **28**, 791-797.

Workman, P. and van Montfort, R. (2014). EML4-ALK fusions: propelling cancer but creating exploitable chaperone dependence. *Cancer Discov* **4**, 642-5.

Yissachar, N., Salem, H., Tennenbaum, T. and Motro, B. (2006). Nek7 kinase is enriched at the centrosome, and is required for proper spindle assembly and mitotic progression. *FEBS Lett* **580**, 6489-95.

Figures

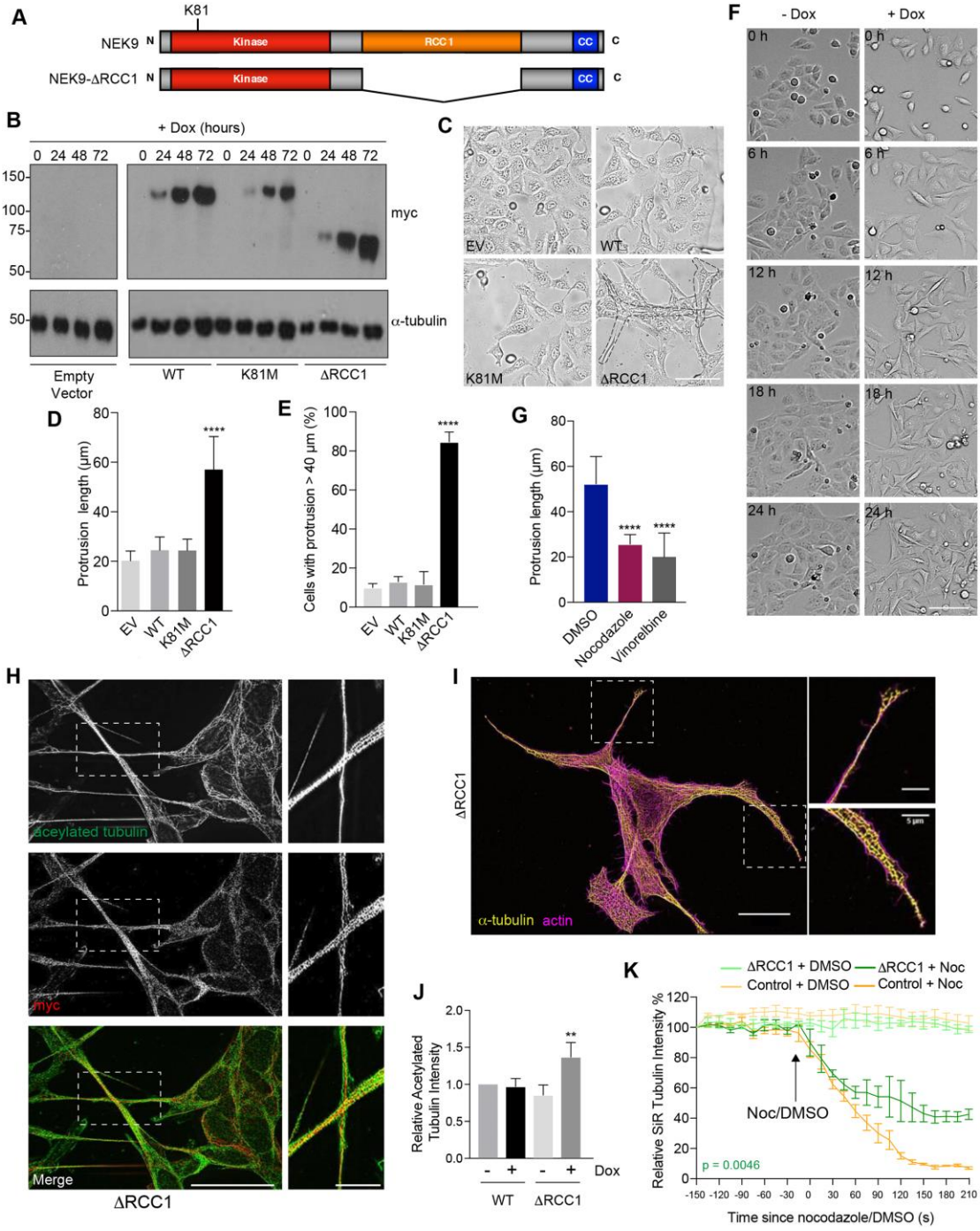

Figure 1. Constitutively active NEK9 induces altered morphology and stabilised microtubules in interphase cells

A. Schematic representation of full-length and activated NEK9 indicating the kinase, RCC1 and coiled-coil (CC) domains. The position of the inactivating K81M mutation is indicated. **B**.

U2OS stable cell lines were induced to express wild-type (WT), catalytically-inactive (K81M) or constitutively-active (ΔRCC1) myc-NEK9 for 0, 24, 48 and 72 h. Lysates were prepared and analysed by Western blot with myc and α-tubulin antibodies. U2OS cells with the tetracycline-inducible plasmid (empty vector, EV) were used as a negative control. **C**. Cells as in B were induced to express Nek9 proteins for 48 h prior to imaging by phase contrast microscopy; scale bar, 50 µm. **D**. The maximum length of cytoplasmic protrusions for cells in C is indicated. **E**. The percentage of cells with protrusions exceeding 40 µm for cells in C & D is indicated. **F**. Stills from time-lapse phase-contrast imaging of U2OS:myc-NEK9-ΔRCC1 cells +/- doxycycline for the times indicated; scale bar, 100 µm. **G**. Dox-Induced U2OS:myc-NEK9-ΔRCC1 were treated with DMSO, nocodazole or vinorelbine, analysed by phase-contrast microscopy and maximum length of cytoplasmic protrusions measured. **H**. U2OS:myc-NEK9-ΔRCC1 cells were analysed by immunofluorescence microscopy with myc and acetylated tubulin antibodies and images reconstructed using SRRF analysis. **I**. U2OS:myc-NEK9-ΔRCC1 cells were analysed by immunofluorescence microscopy with α-tubulin antibodies while actin was stained with phalloidin-FITC. Images were reconstructed using SRRF analysis. In H & I, magnified views of cytoplasmic protrusions are shown on the right from boxed regions in cells on the left. Scale bars, 20 µm (main image) and 5 µm (zooms). **J**. Cell lysates prepared from U2OS:myc-NEK9-WT and ΔRCC1 cells were Western blotted with acetylated tubulin and GAPDH antibodies. The intensity of acetylated tubulin relative to GAPDH is indicated. **K**. U2OS:myc-NEK9-WT and ΔRCC1 cells were incubated with SiR-Tubulin and SiR-Tubulin intensity measured following addition of nocodazole or DMSO.

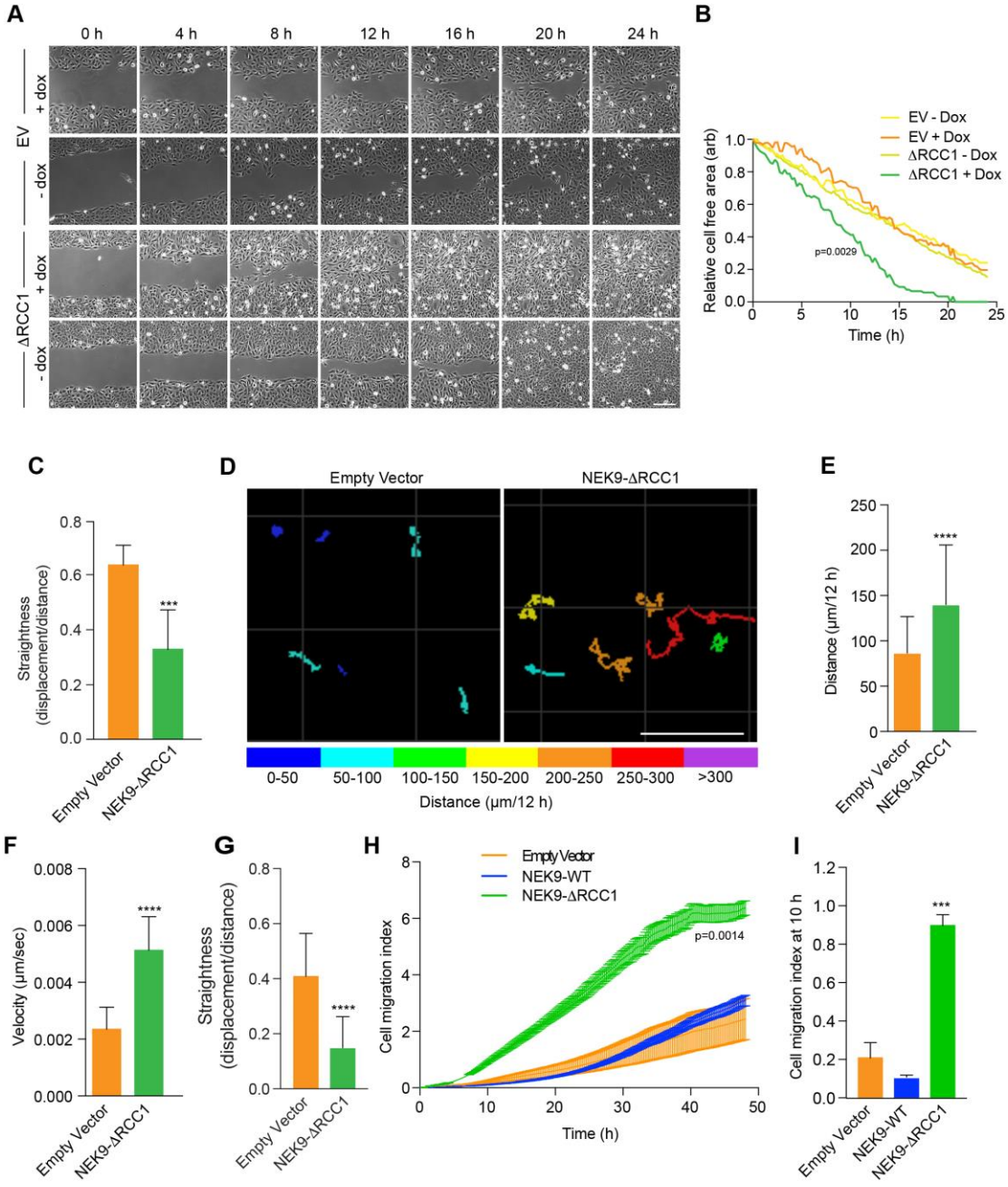

Figure 2. Activated NEK9 disturbs cell polarity and increases cell migration

A. U2OS:myc-NEK9-ΔRCC1 or -EV (empty vector) were imaged to observe closure of a scratch wound. Representative images at time-points indicated are shown; scale bar, 200 μm. **B**. Rates of wound closure for cells in A is shown. **C**. The persistence of movement for cells at the leading edged of the wound generated as in A was measured by quantifying track straightness for each cell. **D**. U2OS:myc-NEK9-ΔRCC1 or –EV were induced for 24 h, transfected with YFP for 24 h and subsequently imaged by time-lapse microscopy. Movement of individual cells was tracked over a 12 h period by following the position of the YFP signal;

distance travelled is colour-coded as indicated (μm). Scale bar, 100 μm. **E**. The mean distance travelled by cells treated as in D is indicated. **F**. The mean velocity of cells treated as in D is indicated. **G**. The persistence of movement for cells in D was measured by quantifying track straightness (track displacement/track length) for each cell. **H**. U2OS:myc-NEK9-WT, -ΔRCC1 or -EV were induced for 24 h before being starved in serum-free medium for a further 24 h, and seeded in RTCA CIM-16 plates. Complete medium containing 10% FBS was used as a chemo-attractant and impedance measurements were used to determine cell migration in real time. **I**. The histogram shows the cell migration index at 10 h from the RTCA assays presented in H.

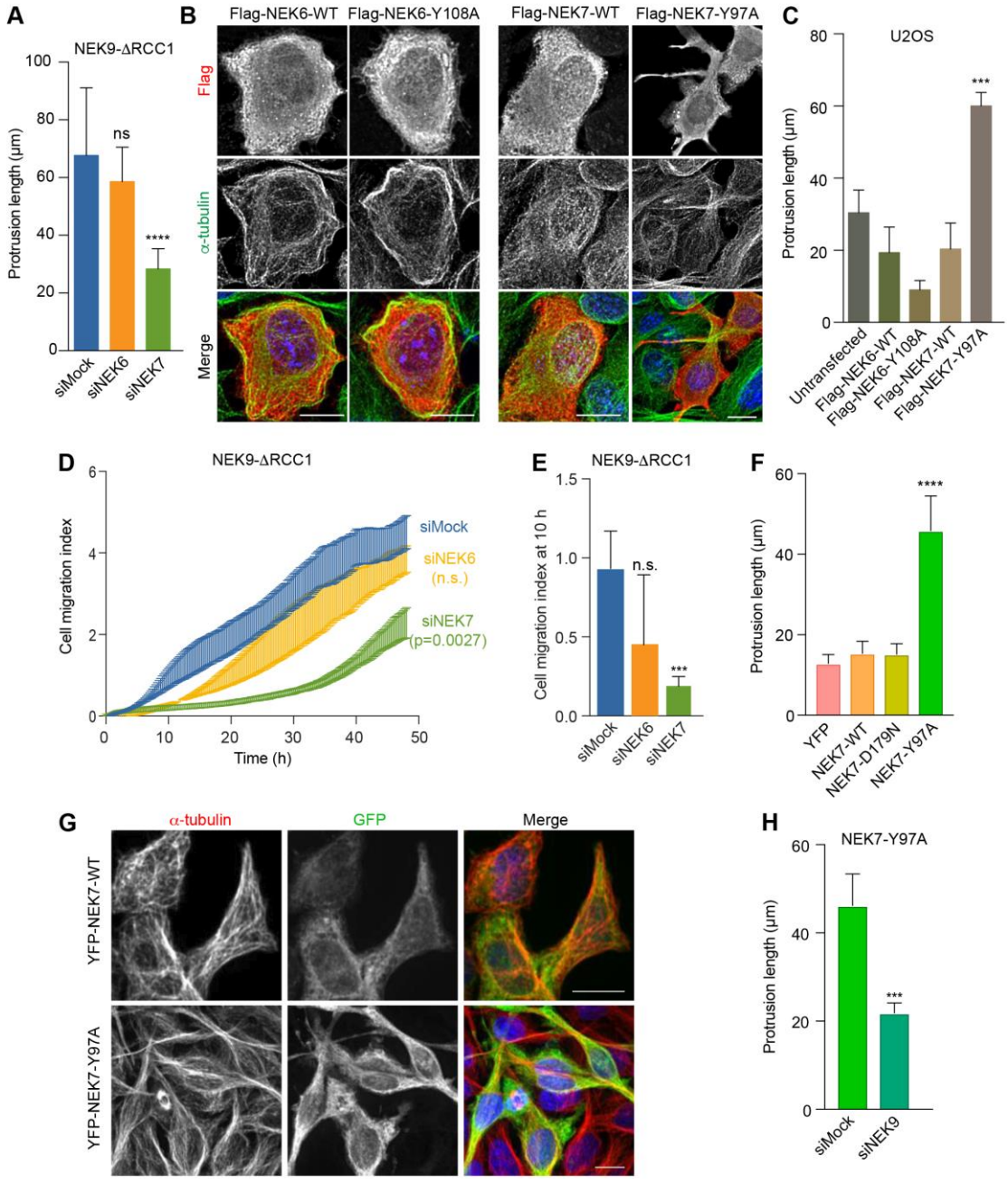

Figure 3. NEK9-induced alterations in cell morphology and migration are dependent on NEK7

A. U2OS:myc-NEK9-ΔRCC1 cells were depleted as indicated. Cells were processed for immunofluorescence microscopy and maximum length of interphase cytoplasmic protrusions measured. **B**. U2OS cells were transiently transfected with wild type (WT) or constitutively active Flag-NEK6 (Y108A) or Flag-NEK7 (Y97A), as indicated, before being processed for immunofluorescence microscopy with Flag (green) and α-tubulin (red) antibodies. DNA (blue) was stained with Hoechst 33258; scale bars, 10 μm. **C**. The maximum length of interphase

cytoplasmic protrusions for cells in B. **D**. U2OS:myc-NEK9-ΔRCC1 cells were depleted, as indicated and cell migration was analysed in real time as in 2H. **E**. Cell migration index at 10 h from the RTCA assays in D. **F**. HeLa:YFP, or YFP-NEK7-WT, D179N or Y97A cells were processed for immunofluorescence microscopy and the maximum length of interphase cytoplasmic protrusions measured. **G**. HeLa:YFP-NEK7-WT and Y97A cells were analysed by immunofluorescence microscopy with GFP (green) and α-tubulin (red) antibodies. Scale bar, 20 µm. **H**. HeLa:YFP-NEK7-Y97A were depleted as indicated and cells were processed for immunofluorescence microscopy and maximum length of interphase cytoplasmic protrusions measured.

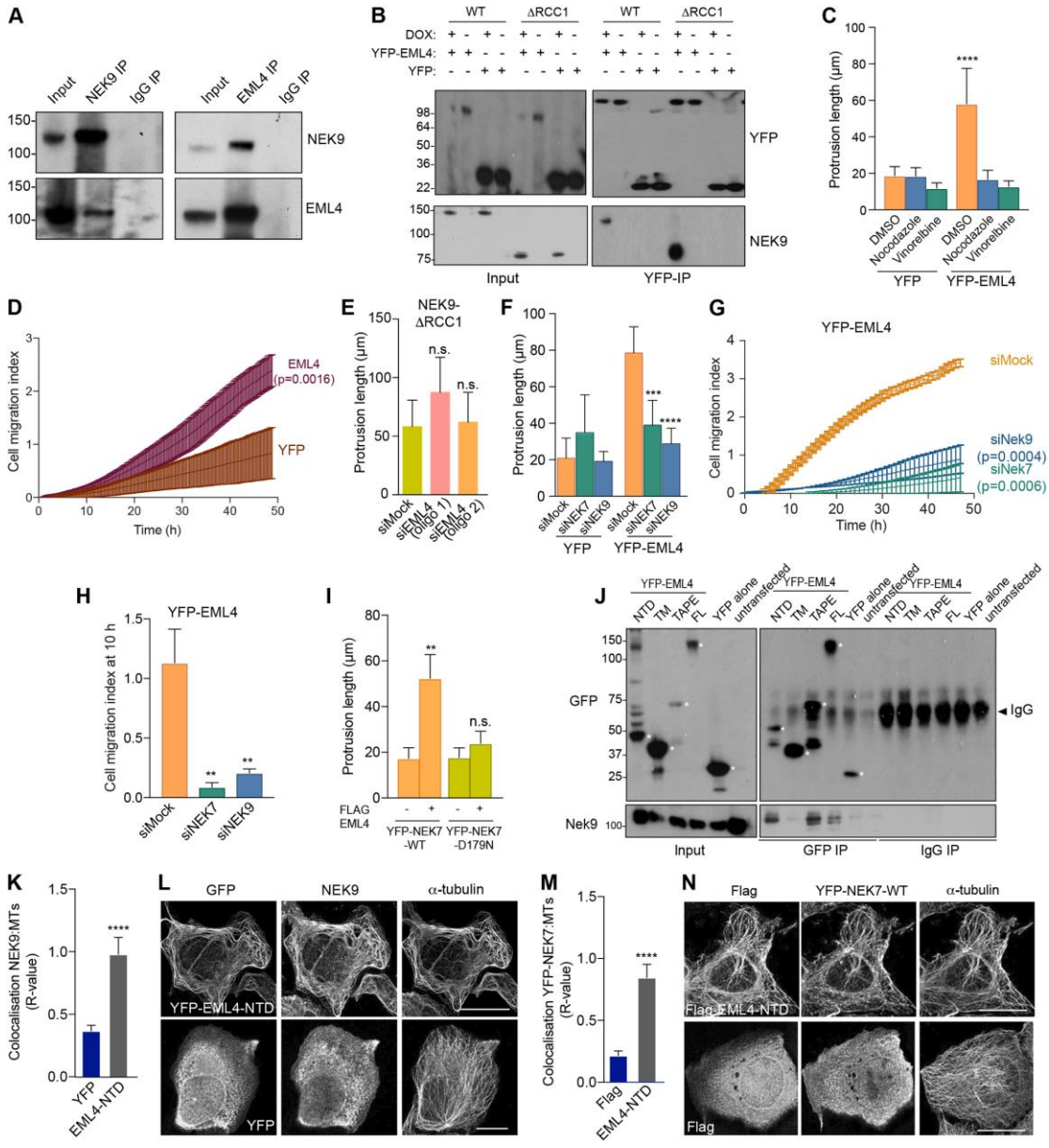

Figure 4. EML4 induces NEK9-dependent changes in cell morphology and migration and recruits NEK9 and NEK7 to interphase microtubules

A. U2OS cell lysates (inputs) and immunoprecipitates (IP) prepared with rabbit NEK9 and control IgGs were analysed by Western blot with antibodies indicated. **B**. U2OS:myc-NEK9-WT or ΔRCC1 cells were transfected with YFP-EML4 or YFP alone. Lysates (input) and Immunoprecipitates (IP) were prepared with GFP antibodies and analysed by Western blot with antibodies indicated. **C**. U2OS:YFP or U2OS:YFP-EML4 cell lines were treated as indicated for 16 h before analysis by phase contrast microscopy and maximum length of interphase cytoplasmic protrusions measured. **D**. Cell migration of U2OS:YFP or U2OS YFP-

EML4 cells was analysed in real time as in Fig. 2H. **E**. U2OS:myc-NEK9-ΔRCC1 were depleted with mock or two different siRNAs against EML4 and the maximum length of interphase cytoplasmic protrusions measured. **F**. U2OS:YFP or U2OS:YFP-EML4 cells were depleted as indicated before being analysed by phase contrast microscopy and the maximum length of interphase cytoplasmic protrusions measured. **G**. U2OS:YFP-EML4 cells were depleted as indicated and cell migration was analysed in real time as in Fig. 2H. **H**. Cell migration index at 10 h from the data in G. **I**. HeLa:YFP-NEK7-WT or D179N were transfected with Flag-EML4 for 24 h and maximum length of cytoplasmic protrusions for transfected cells measured. **J**. U2OS cells were transfected with YFP-EML4-full length (FL), TM (trimerisation motif), TAPE, NTD or YFP alone for 24 h. Lysates (inputs) and immunoprecipitates (IP) were prepared with GFP and control IgGs and analysed by Western blot with the antibodies indicated. Asterisks indicate the proteins of interest. **K**. U2OS cells were transfected with YFP alone or YFP-EML4 NTD before being processed for immunofluorescence microscopy with antibodies against GFP, NEK9 and α-tubulin, and colocalization between the Nek9 and α-tubulin signal calculated. **L.** Representative images of cells in K. Scale bar, 10 µm. **M**. HeLa:YFP-NEK7 cells were transfected with flag alone or Flag-EML4-NTD for 24 h. Cells were processed for immunofluorescence microscopy with antibodies against Flag, GFP and α-tubulin. Co-localization between the YFP-NEK7 fluorescence and α-tubulin signal was calculated. **N**. Representative images of cells in M. *R* values in B and D show the mean Pearson's correlation coefficient from 5 lines per cell in 10 cells (±S.D.).

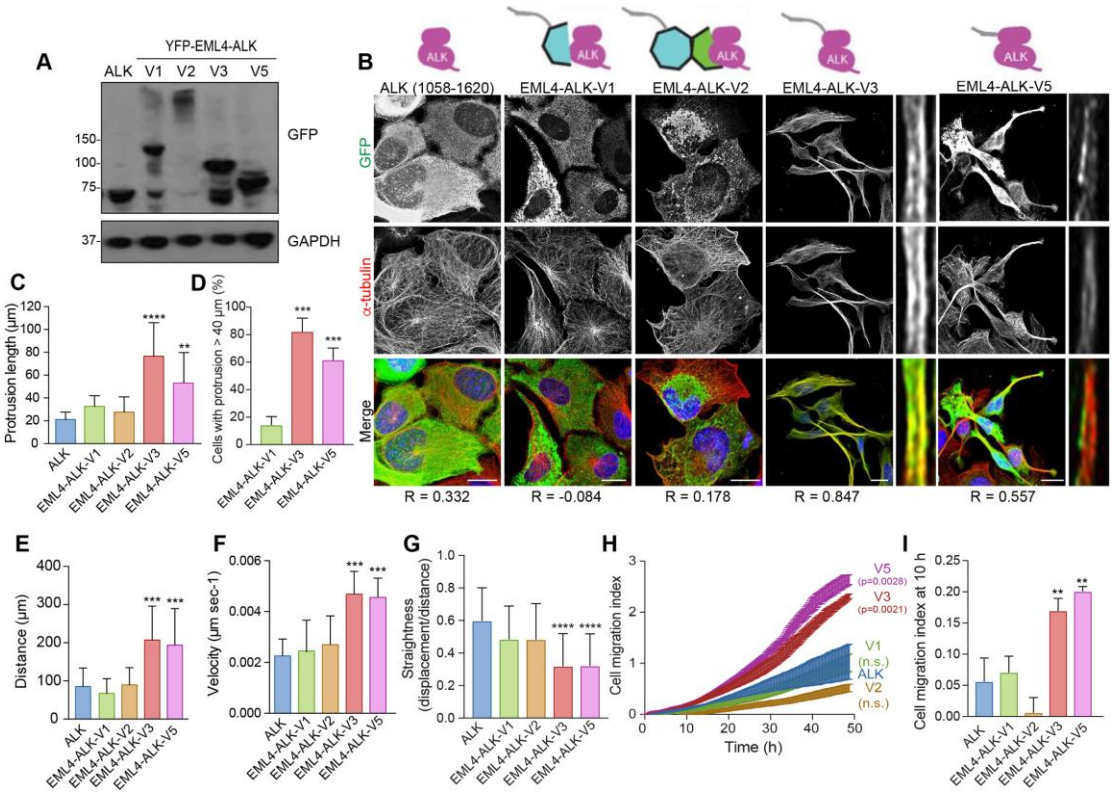

Figure 5. EML4-ALK variants that bind microtubules alter cell morphology and migration

A. U2OS cell lines stably expressing YFP-tagged EML4-ALK fusion variants were lysed and analysed by Western blot with antibodies indicated. **B**. U2OS stable cell lines expressing YFP-tagged proteins as in A were analysed by immunofluorescence microscopy with antibodies against GFP (green) and α-tubulin (red). DNA (blue) was stained with Hoechst 33258. Magnified views of individual microtubules are shown on the right of V3 and V5 images shown on the left. Schematic versions of the YFP-tagged proteins and the Pearson's correlation coefficient (*R*) of co-localization with microtubules are shown. Scale bars, 10 μm. **C**. The maximum length of interphase cytoplasmic protrusions for cells in B. **D**. The % of cells from B and C with protrusions greater than 40 μm is indicated. **E**. Individual cell tracking experiments were undertaken with cell lines as in A and analysed as in Fig. 2D. The mean distance travelled is indicated. **F.** As for E, but showing mean velocity of movement. **G**. As for E but showing track straightness. **H**. Migration of cells as in A was analysed in real time as in Fig. 2H. **I**. The cell migration index at 10 h from the data in H.

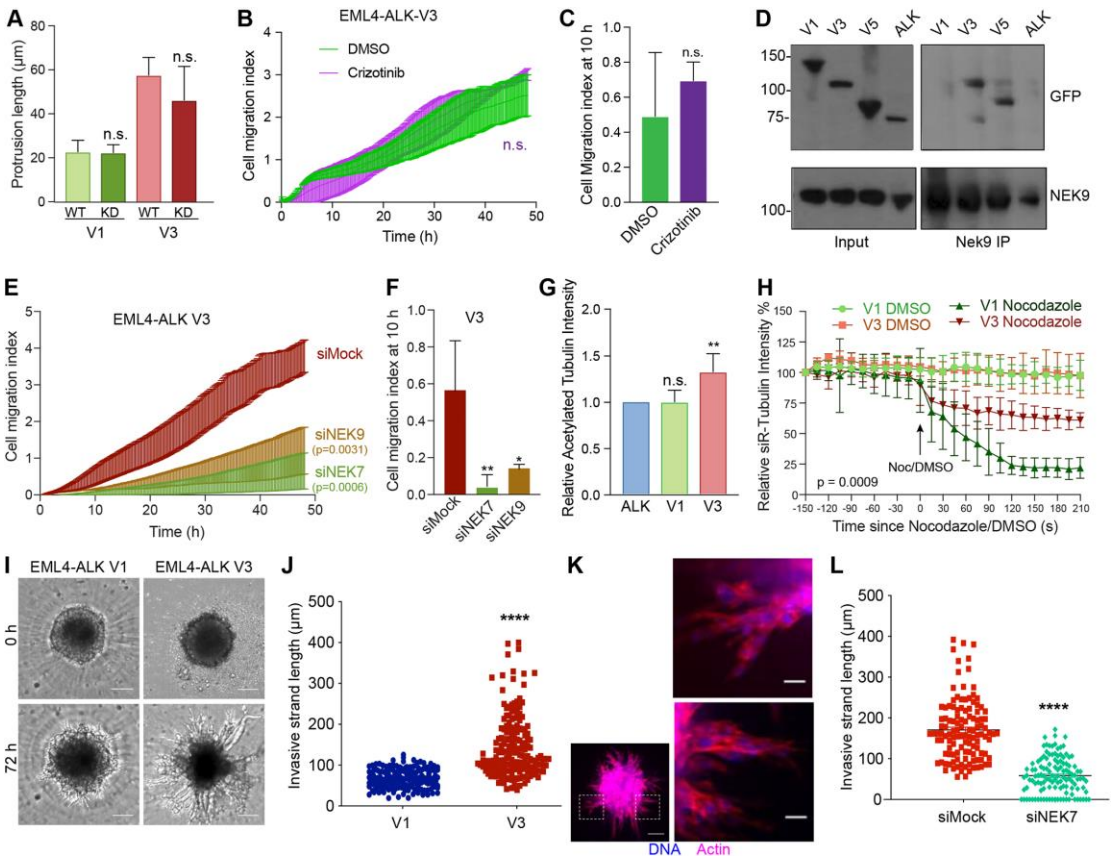

Figure 6. EML4-ALK V3 disturbs cell polarity, stabilises microtubules and binds NEK9

A. U2OS cells were transfected with WT and Kinase Dead (KD) YFP-EML4-ALK-V1 and V3, as indicated, and analysed by immunofluorescence microscopy. The maximum length of interphase cytoplasmic protrusions for transfected cells was measured. **B**. U2OS:YFP-EML4-ALK-V3 cells were treated with DMSO or 100 nM Crizotinib and cell migration analysed in real time as in Fig. 2H. **C**. Cell migration index at 10 h from data in B. **D**. U2OS:YFP-EML4-ALK cells, as indicated, were lysed and lysates (inputs) and immunoprecipitates (IP) prepared with NEK9 antibodies or control IgGs analysed by Western blot with the antibodies indicated. **E**. U2OS:YFP-EML4-ALK-V3 cells were mock-, NEK6- or NEK7-depleted and cell migration analysed in real time as in Fig. 2H. **F**. Cell migration index at 10 h from data in E. **G**. Cell lysates prepared from U2OS:YFP-EML4-ALK-V1 and V3 cells were Western blotted with acetylated tubulin and GAPDH antibodies and the intensity of acetylated tubulin plotted relative to GAPDH. **H**. U2OS:YFP-EML4-ALK-V1 and V3 were incubated with SiR-Tubulin and SiR-Tubulin intensity measured following addition of nocodazole. Control cells were treated with DMSO. **I**. Phase-contrast microscopy of invasion into Matrigel of dox-induced Beas-2B:EML4-ALK V1 and V3 at timepoints indicated. Scale bar, 100 μm **J**. Length of invasive strand after 72 h for cells in I. **K**. Cells were treated as in I but fixed and actin stained with TRITC-phalloidin (red) and DNA with Hoechst 33258 (blue). Magnified views of chains of cells are shown on the right from the boxed regions of the spheroid on the left.

Scale bars, 20 µm (zooms), 100 µm (whole image) **L**. EML4-ALK V3 cells were treated as in I except cells were also transfected with Nek7 siRNAs and length of invasive strand measured.

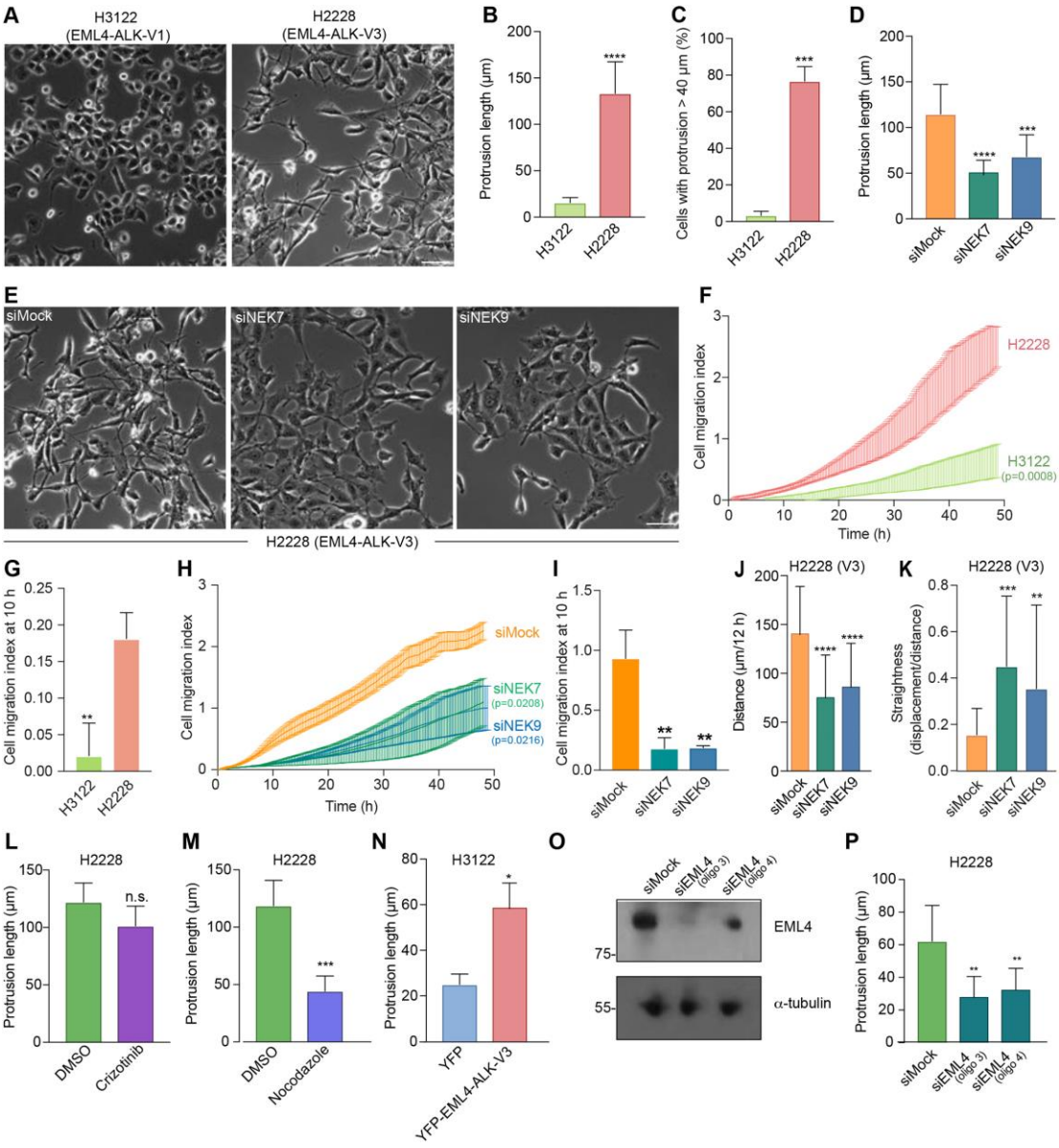

Figure 7. Depletion of NEK7 or NEK9 reduces migration of NSCLC patient cells expressing microtubule-binding EML4-ALK variants

A. H3122 and H2228 cells were analysed by phase contrast microscopy. **B**. Maximum length of interphase cytoplasmic protrusions for each cell type. **C**. The % of cells from A and B with protrusions greater than 40 µm is indicated. **D**. H2228 cells were depleted with NEK7 or NEK9 siRNAs and the maximum length of cytoplasmic protrusions measured. **E** Phase contrast images of cells treated in D. **F**. H3122 and H2228 cell migration was analysed in real time as in Fig. 2H. **G**. Cell index at 10 h for cells in F is shown. **H**. H2228 cells were depleted as indicated and migration analysed in real time as in Fig. 2D. **I**. Cell migration index at 10 h for cells in H is shown. **J** & **K**. H2228 cells that were mock- or NEK9-depleted were analysed by individual cell tracking as in Fig. 2D. Mean distance travelled (J) and track straightness (K) is shown. **L** & **M**. H2228 cells were treated with crizotinib (L) or nocodazole (M) and the

maximum length of interphase cytoplasmic protrusions measured, control cells were treated with DMSO. **N**. H3122 cells were transfected with either YFP alone or YFP-EML4-ALK V3 and the maximum length of interphase cytoplasmic protrusions for transfected cells measured. **O**. Lysates were prepared from H2228 cells that were mock transfected or transfected with two alternative siRNAs (siEML4 #3 & 4) designed to target the portion of EML4 found in the EML4-ALK-V3 expressed in H2228 cells and Western blotted as indicated. **P**. Maximum length of interphase cytoplasmic protrusions for cells treated as in O. Scale bars in A, and D, 100 µm.

A

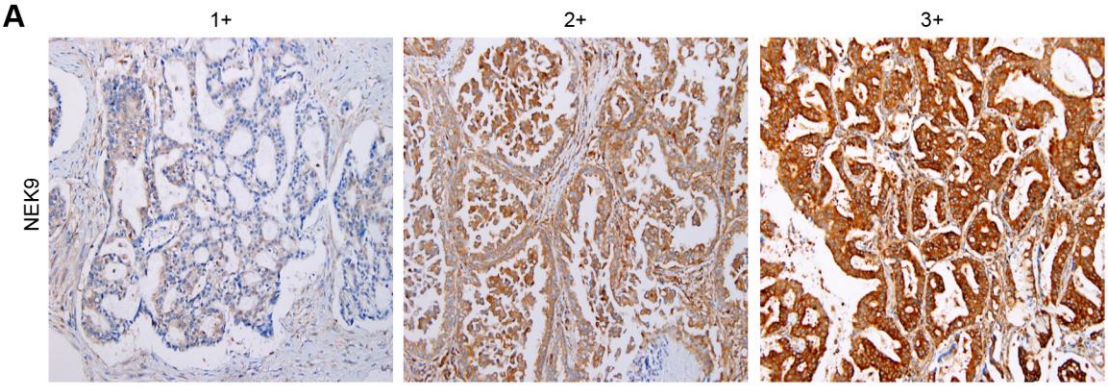

B

EML4-ALK Variant	NEK9 score		Total	p value
	1+	2+/3+		
V1/2/others	16	9	25	
V3/5	2	20	22	<0.001
Total	18	29	47	

C

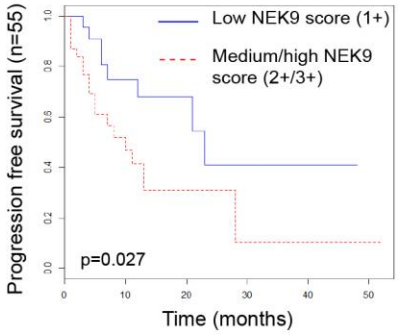

D

(i) EML4-ALK V1/V2
Low NEK9

(ii) EML4-ALK V3/V5
High NEK9

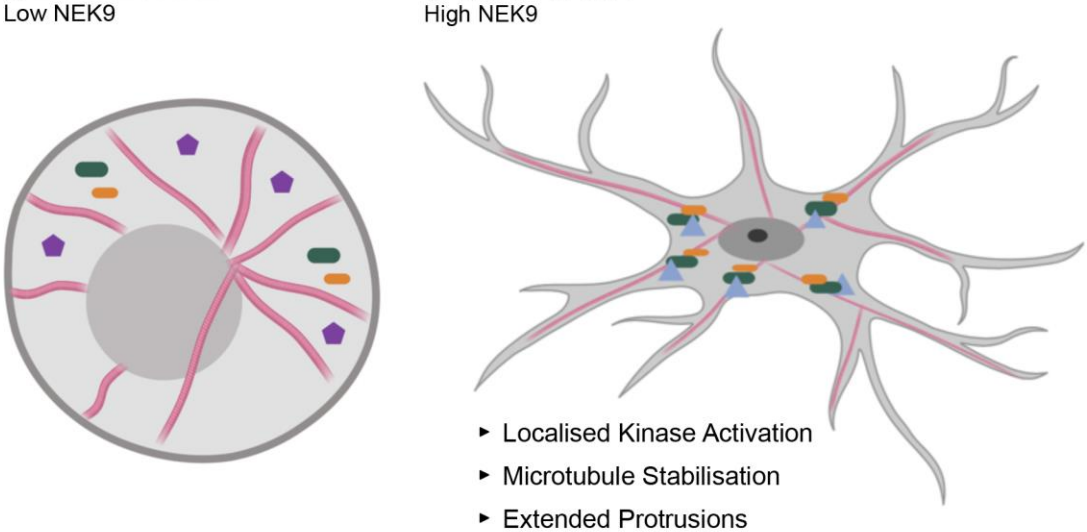

- Localised Kinase Activation
- Microtubule Stabilisation
- Extended Protrusions
- Enhanced Migration

Figure 8. Elevated NEK9 expression correlates with EML4-ALK V3/V5 genotype in NSCLC patient tumours as well as poor overall survival

A. Tumour biopsies from NSCLC patients were processed for immunohistochemistry with NEK9 antibodies (brown) and scored as low (1+), medium (2+) or high (3+). Tissue was also stained with haematoxylin to detect nuclei (blue). **B.** Table indicates NEK9 expression as determined as in A with respect to the EML4-ALK variant present. **C.** The Kaplan-Meier plot indicates progression-free survival of NSCLC patients with EML4-ALK fusion that had low (1+) or medium/high (2+/3+) NEK9 expression (n=32). **D.** Schematic model showing rationale for stratification of cancer patients for treatment based on EML4-ALK variant. (i) The majority of tumours expressing EML4-ALK V1/V2 express low levels of NEK9. In these cells, the EML4-ALK protein neither binds NEK9 nor colocalises with microtubules, and cells retain a more rounded morphology. (ii) However, the majority of tumours expressing EML4-ALK V3/V5 express moderate or high levels of NEK9. In these cells, the EML4-ALK protein binds and recruits NEK9 and NEK7 to microtubules leading to localised kinase activity that promotes microtubule stabilization, extended cytoplasmic protrusions and enhanced migration.

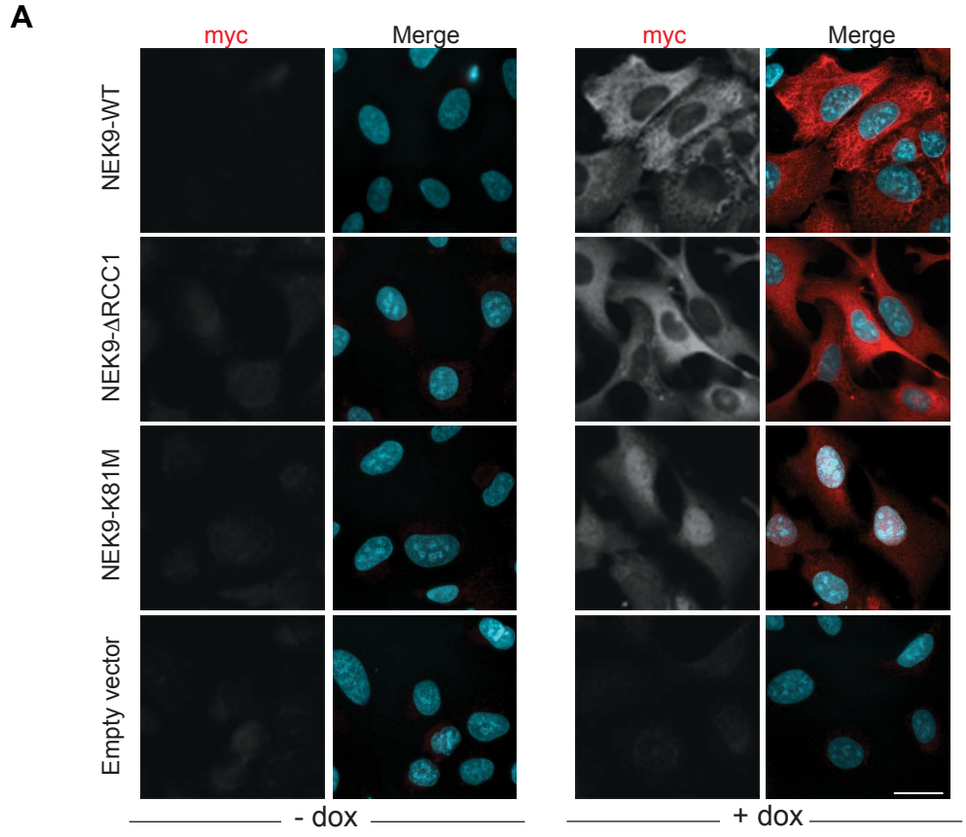

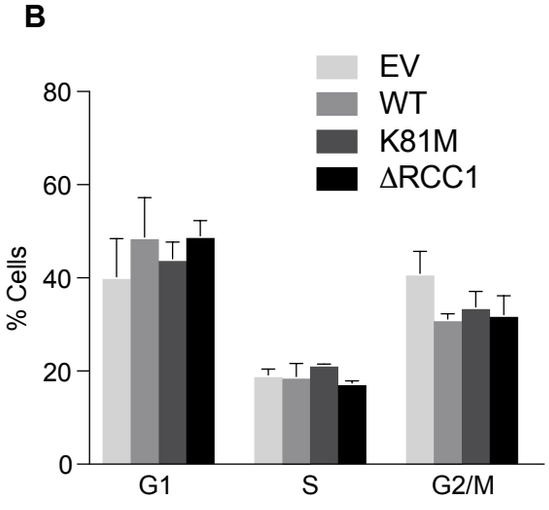

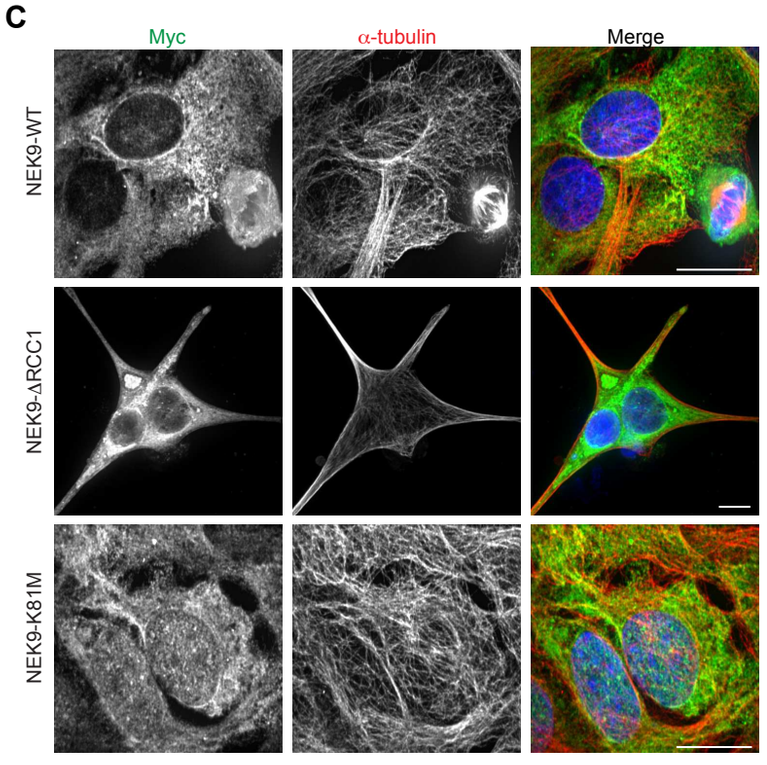

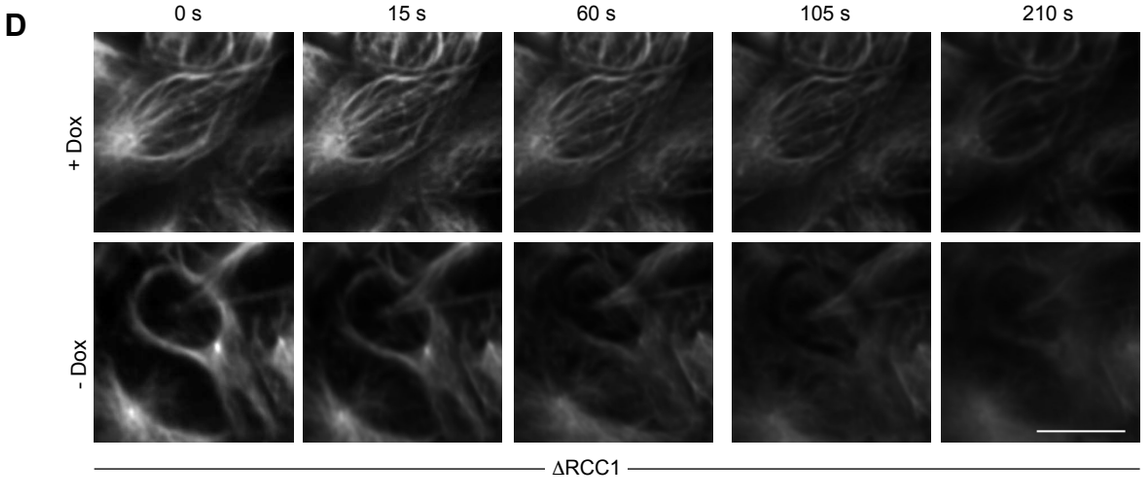

Figure S1. Characterisation of doxycycline-inducible U2OS:myc-NEK9 constructs

A. U2OS:myc-NEK9-WT, ΔRCC1 or K81M cells, or cells containing empty vector, were either uninduced (- dox) or induced (+ dox) for 72 h before being processed for immunofluorescence microscopy with myc (red) antibodies. **B**. U2OS:myc-NEK9-WT, ΔRCC1 or K81M cells were induced for 72 h before being fixed, stained with propidium iodide and analysed by flow cytometry. The percentage of cells in G1, S and G2/M are indicated. **C.** Cells were treated as in A and analysed by immunofluorescence microscopy with myc (green) and α-tubulin (red) antibodies. In A & C, DNA was stained with Hoechst 33258 (blue); scale bars, 20 μm. **D**. U2OS:myc-NEK9-ΔRCC1 cells were treated for 48 hours +/- doxycycline before incubation with SiR-Tubulin to visualise microtubules. SiR-Tubulin intensity was then measured every 15 s following addition of nocodazole. Stills from movies are shown. Scale bar, 10 μm.

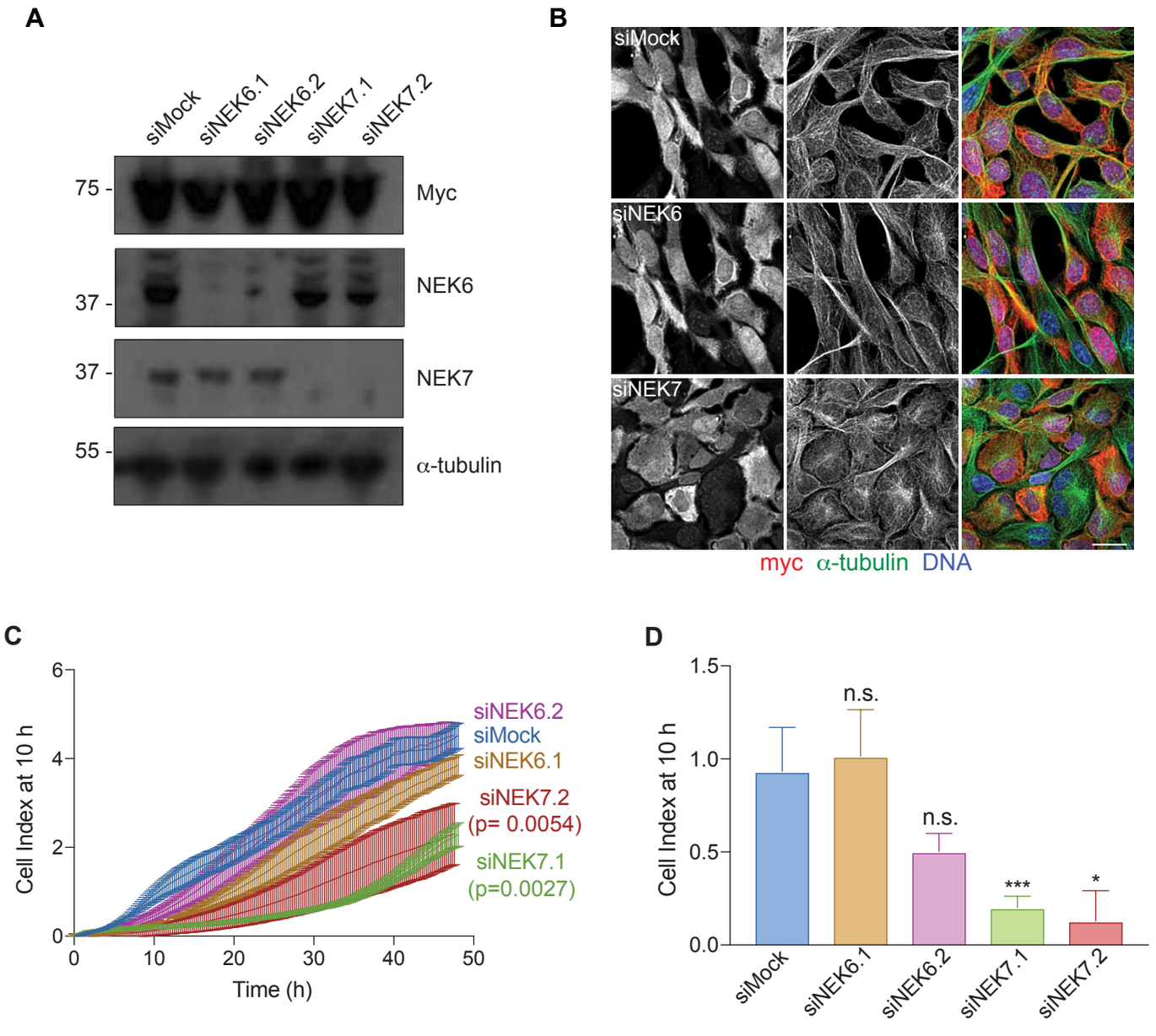

Figure S2. Depletion of NEK6 and NEK7 in NEK9-ΔRCC1 cell lines

A. U2OS:myc-NEK9-ΔRCC1 cells were mock-depleted or depleted with NEK6 or NEK7 siRNAs for 24 h prior to induction with doxycycline for a further 48 h. Cell lysates were prepared and analysed by Western blot with myc, NEK6, NEK7 and α-tubulin antibodies. **B**. U2OS:myc-NEK9-ΔRCC1 cells were mock-depleted, or depleted with siNEK6.1 or siNEK7.1 and processed for immunofluorescence microscopy with myc (red) and α-tubulin (green) antibodies. DNA was stained with Hoechst 33258. Scale bar, 20 μm. **C**. U2OS:myc-NEK9-ΔRCC1 cells were treated as in A and analysed using the live cell transwell migration assay. Data represent means from 3 separate experiments. **D**. Histogram shows the cell migration index at 10 h based on data in C.

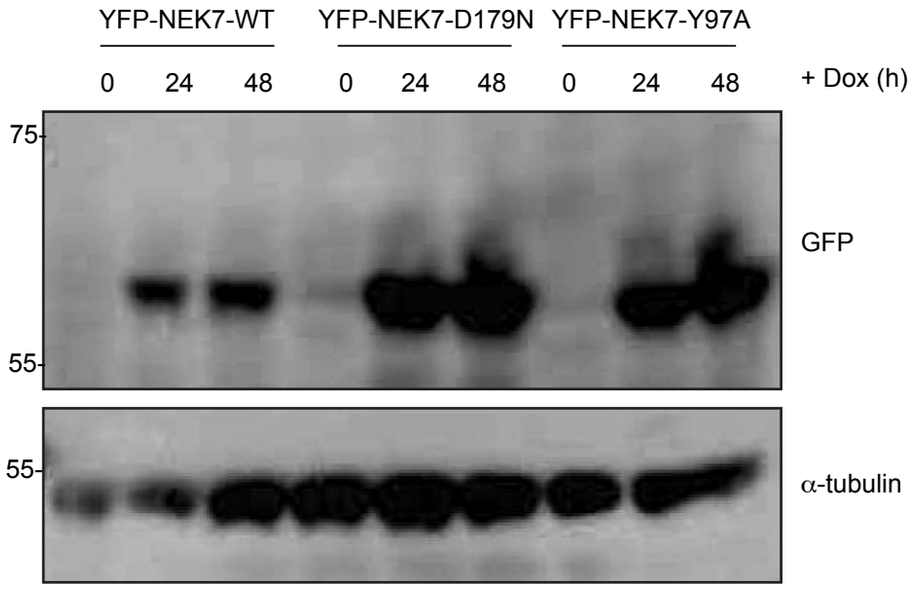

Figure S3. Characterisation of doxycycline-inducible HeLa:YFP-NEK7 constructs

Lysates prepared from HeLa stable cell lines induced to express wild-type (WT), catalytically-inactive (D179N) or constitutively-active (Y97A) YFP-NEK7 with doxycycline for 0, 24 and 48 h were analysed by Western blot with GFP and α-tubulin antibodies. M. wts (kDa) are indicated on the left.

A

Probablilty legend:

Over 95 %
80-94 %
50-79 %
20-49 %
0-19 %

UL00825GB				Control	Nek9
#	Identified Proteins (3)	Accession Numbe	Molecular Weight	UL00825GB - 02 - Con	UL00825GB - 01 - Nek9
1	Serine/threonine-protein kinase Nek9 OS=Homo sapiens GN=NEK9 PE=1 SV=2	Q8TD19	107 kDa	!	29
2	Echinoderm microtubule-associated protein-like 4 OS=Homo sapiens GN=EML4 PE=1 SV=3	Q9HC35	109 kDa	0	8

B

Sequence	Scaffold Probability	Mascot Ion score	Mascot Identity score	X! Tandem	Observed	Actual Mass	Charge	Delta Da	Delta PPM
(K)DVIINQEGEYIK(M)	100%	29.2	22.4	3.72	710.8697	1419.7248	2	0.0001	0.04
(R)TELPPEK(L)	100%	28.6	18.6	1.82	407.2213	812.4280	2	-0.0002	-0.27
(R)IATGQIAGVDK(D)	100%	31.1	21.8	2.52	536.8033	1071.5921	2	-0.0006	-0.57
(R)GVGcLDFSK(A)	100%	33.4	19.1	0.96	491.7368	981.4591	2	0.0000	-0.03
(K)TTVEPTPGK(G)	98%	30.7	20.5		465.2505	928.4864	2	-0.0004	-0.43
(R)EIEVPDQYGTIR(A)	99%	20.0	22.2	1.09	710.3607	1418.7068	2	0.0024	1.68
(R)WFVLDAETR(D)	100%	37.0	21.9	2.08	568.7901	1135.5657	2	-0.0006	-0.51
(K)LSLPQNETVADTTLTK(A)	100%	31.8	21.9	3.10	865.9627	1729.9109	2	0.0008	0.46

C

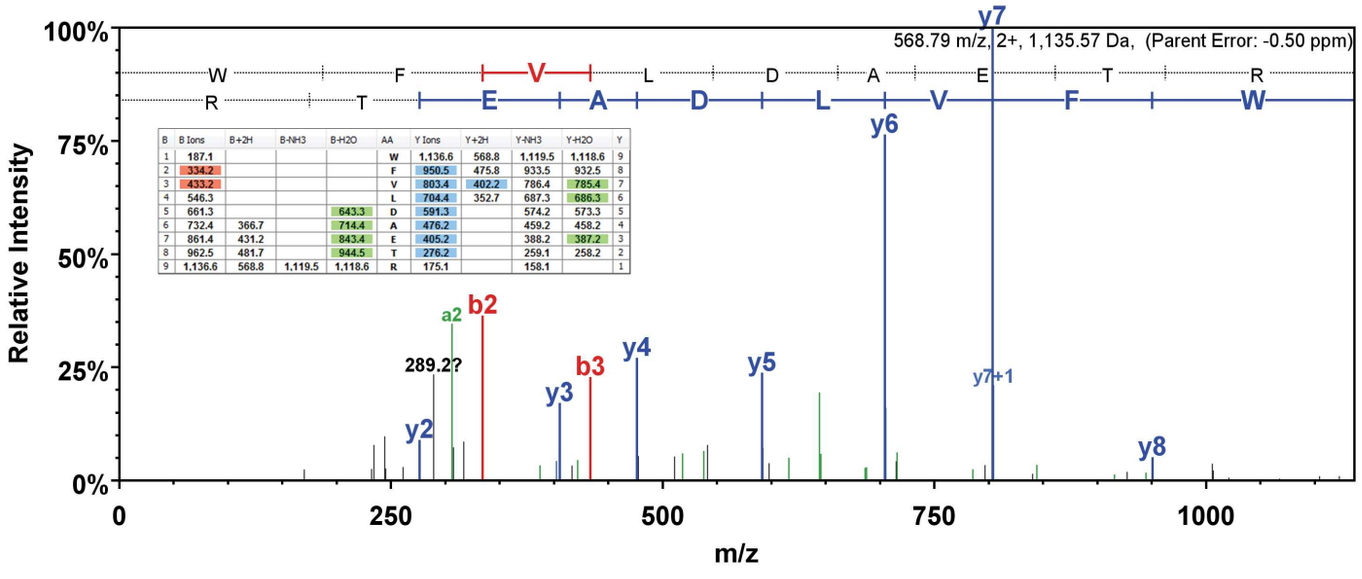

B	B Ions	B+2H	B-NH3	B-H2O	AA	Y Ions	Y+2H	Y-NH3	Y-H2O	Y
1	187.1				W	1,136.6	568.8	1,119.5	1,118.6	9
2	334.2				F	950.5	475.8	933.5	932.5	8
3	433.2				V	803.4	402.2	786.4	785.4	7
4	546.3				L	704.4	352.7	687.3	686.3	6
5	661.3			643.3	D	591.3		574.2	573.3	5
6	732.4	366.7		714.4	A	476.2		459.2	458.2	4
7	861.4	431.2		843.4	E	405.2		388.2	387.2	3
8	962.5	481.7		944.5	T	276.2		259.1	258.2	2
9	1,136.6	568.8	1,119.5	1,118.6	R	175.1		158.1		1

Figure S4. Identification of EML4 as a NEK9 binding partner by mass spectrometry

A. Anti-myc immunoprecipitates prepared from U2OS:myc-NEK9-WT cells induced with doxycycline for 48 hours were analysed by SDS-PAGE and mass spectrometry. Eight peptides representing EML4 were identified in the immunoprecipitates from myc-NEK9 expressing cells, whereas no EML4 peptides were identified in immunoprecipitates from parental U2OS cells. **B**. The table shows peptides identified from human EML4 by LC-MS/MS. **C**. MS/MS spectrum of peptide WFVLDAETR; y-ion fragments highlighted in blue, b-ion fragments in red. Inset shows full fragmentation table.

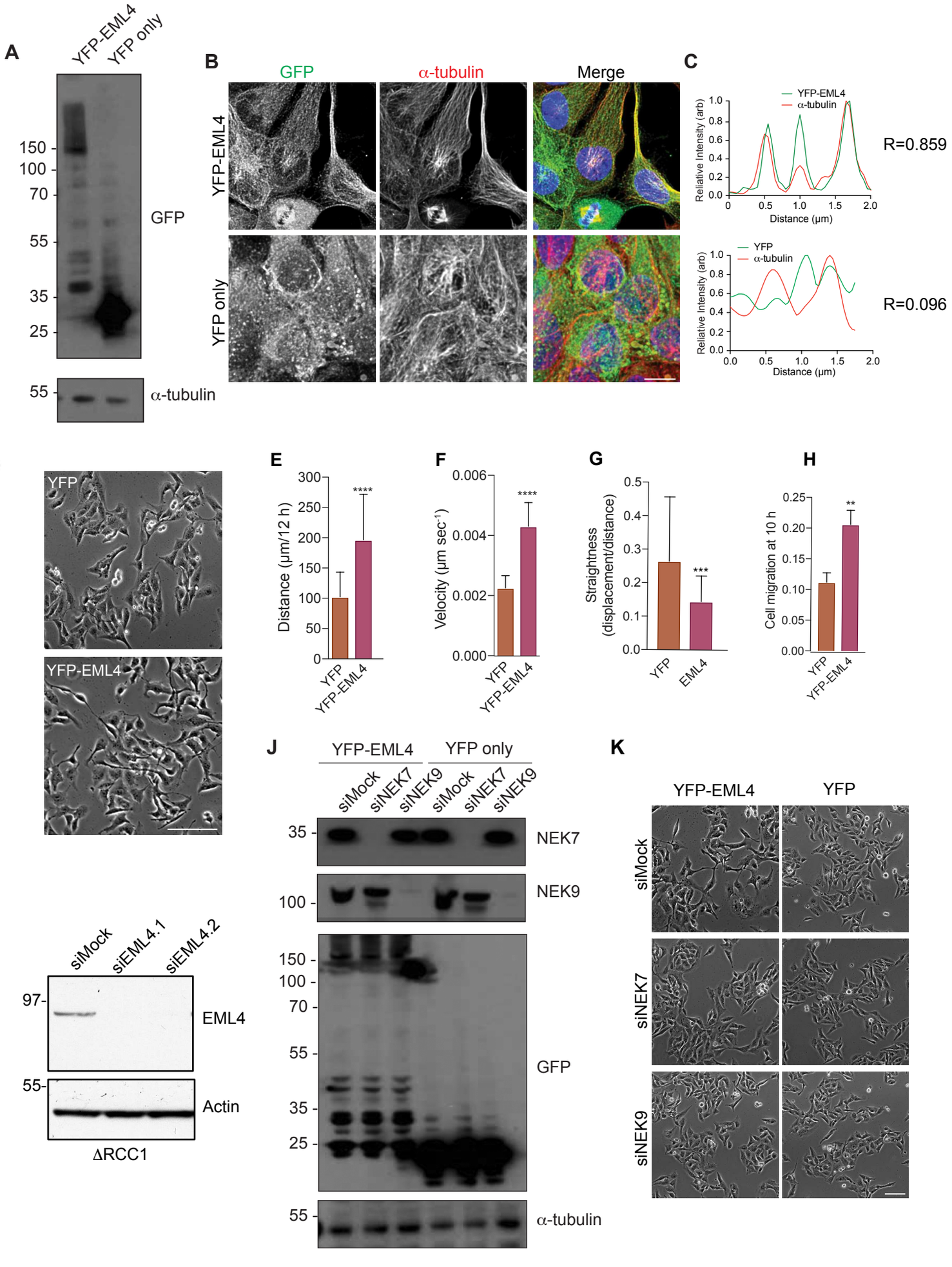

Figure S5. Characterization of U2OS:YFP and U2OS:YFP-EML4 stable cell lines

A. Lysates prepared from U2OS:YFP and U2OS:YFP-EML4 cell lines were Western blotted with the antibodies indicated. **B**. Immunofluorescence microscopy images of U2OS:YFP and U2OS:YFP-EML4 cell lines stained with GFP (green) and α-tubulin (red) antibodies. DNA (blue) is stained with Hoechst 33258. Scale bar, 20 μm. **C**. Representative intensity profiles along a single line-scan showing co-localization of YFP or YFP-EML4 with microtubules. *R* values show the mean Pearson's correlation coefficient from 10 cells. **D**. Phase contrast microscopy of U2OS:YFP and U2OS:YFP-EML4 cell lines. Scale bar, 100 μm. **E**. Individual cell tracking experiments were undertaken with U2OS:YFP and U2OS:YFP-EML4 cell lines and analysed as in Fig. 2D. The mean distance travelled is indicated. **F**. The mean velocity of cells treated as in E is indicated. **G**. The track straightness of cells treated as in E is indicated. **H**. The histogram shows the cell migration index at 10 h from the data in Fig 4D. **I**. Lysates prepared from U2OS:myc-NEK9-ΔRCC1 cells depleted for EML4 with two siRNAs or mock-depleted for 24 h prior to induction with doxycycline for a further 48 h were analysed by Western blot for endogenous EML4 and actin. **J**. Lysates prepared from U2OS:YFP and U2OS:YFP-EML4 cells, which had been depleted for NEK7 or NEK9 or mock depleted for 72 h, were Western blotted for NEK7, NEK9, GFP or α-tubulin. **K**. U2OS:YFP or U2OS:YFP-EML4 cell lines were depleted of NEK7 or NEK9, as indicated, before analysis by phase contrast microscopy; scale bar, 100 μm. M. wts (kDa) are indicated on the left in A, E and F.

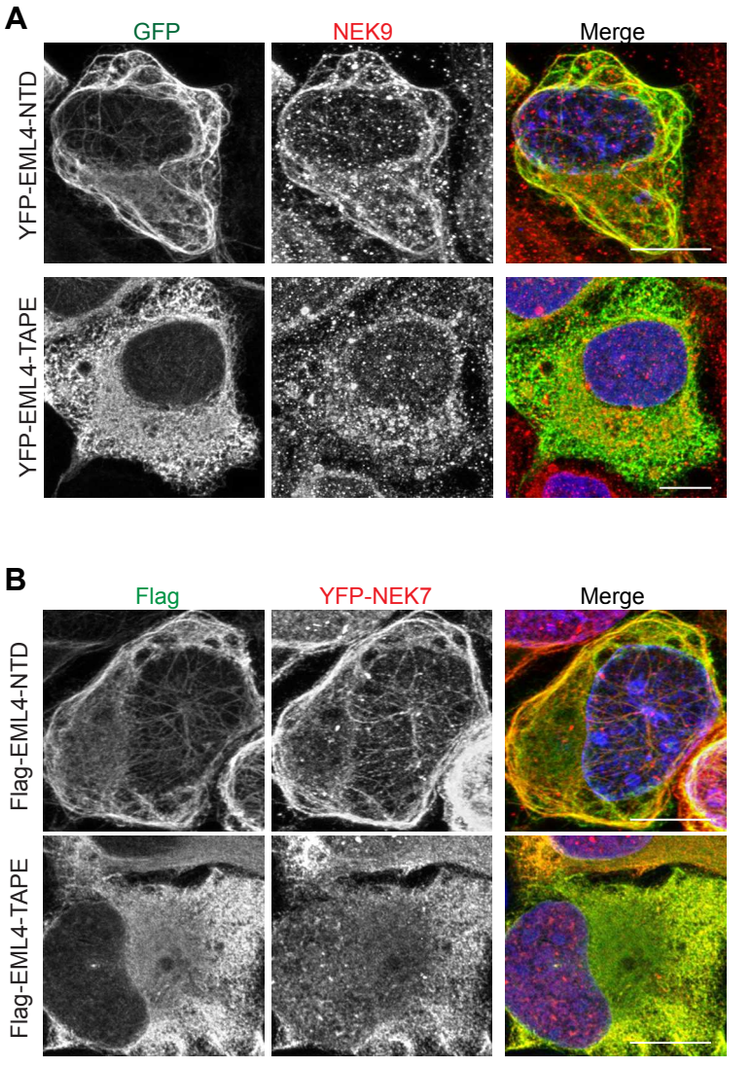

Figure S6. EML4-NTD recruits NEK9 and NEK7 to microtubules

A. U2OS cells were transfected with YFP-EML4 N-terminal domain (NTD) or TAPE domain (TAPE), as indicated, for 24 h before being processed for immunofluorescence microscopy with antibodies against GFP (green) and NEK9 (red). **B**. HeLa:YFP-NEK7 cells were induced for 48 h with doxycycline before being mock transfected or transfected with Flag-EML4-NTD or TAPE for a further 24 h. Cells were then processed for immunofluorescence microscopy with antibodies against Flag (green) and GFP (red). Merge images include DNA stained with Hoechst 33258 (blue). Scale bars, 10 μm.

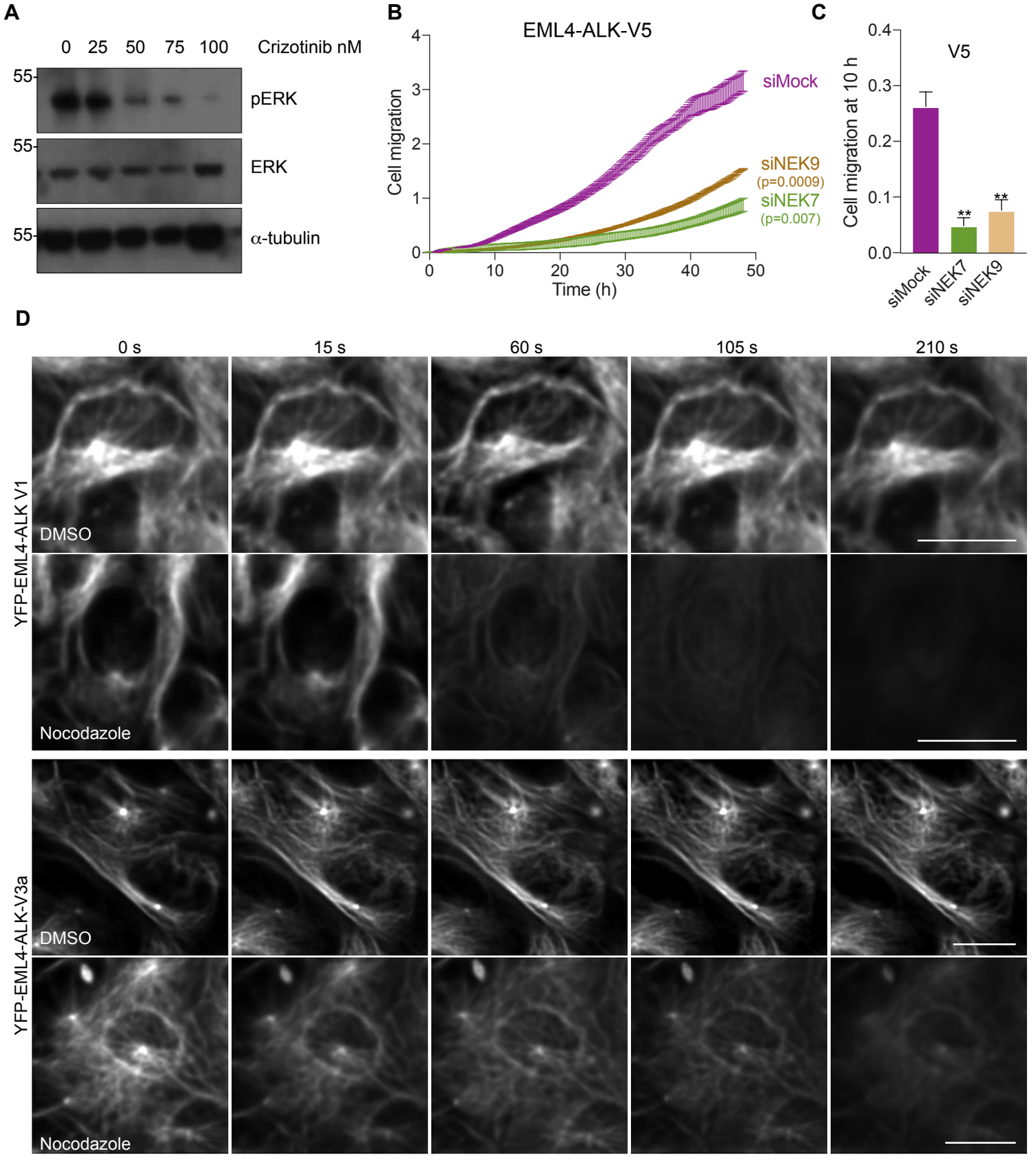

Figure S7. Inhibition of ERK phosphorylation by crizotinib and stabilization of microtubules in EML4-ALK V3 cells

A. Cell lysates prepared from U2OS:YFP-EML4-ALK-V3 cells treated with DMSO or Crizotinib at the concentrations indicated for 8 h were analysed by Western blot with ERK, pERK and α-tubulin antibodies. **B**. . U2OS:YFP-EML4-ALK-V3 cells were mock-, NEK6- or NEK7-depleted for 72 h and cell migration analysed in real time as in Fig. 2M. **C**. The histogram shows the cell migration index at 10 h from data in B. **D**. U2OS:YFP-EML4-ALK V1 or V3 cells were incubated with SiR-Tubulin to visualise microtubules before SiR-Tubulin intensity was measured every 15 s following addition of DMSO or nocodazole. Stills from movies are shown. Scale bars, 10 µm.

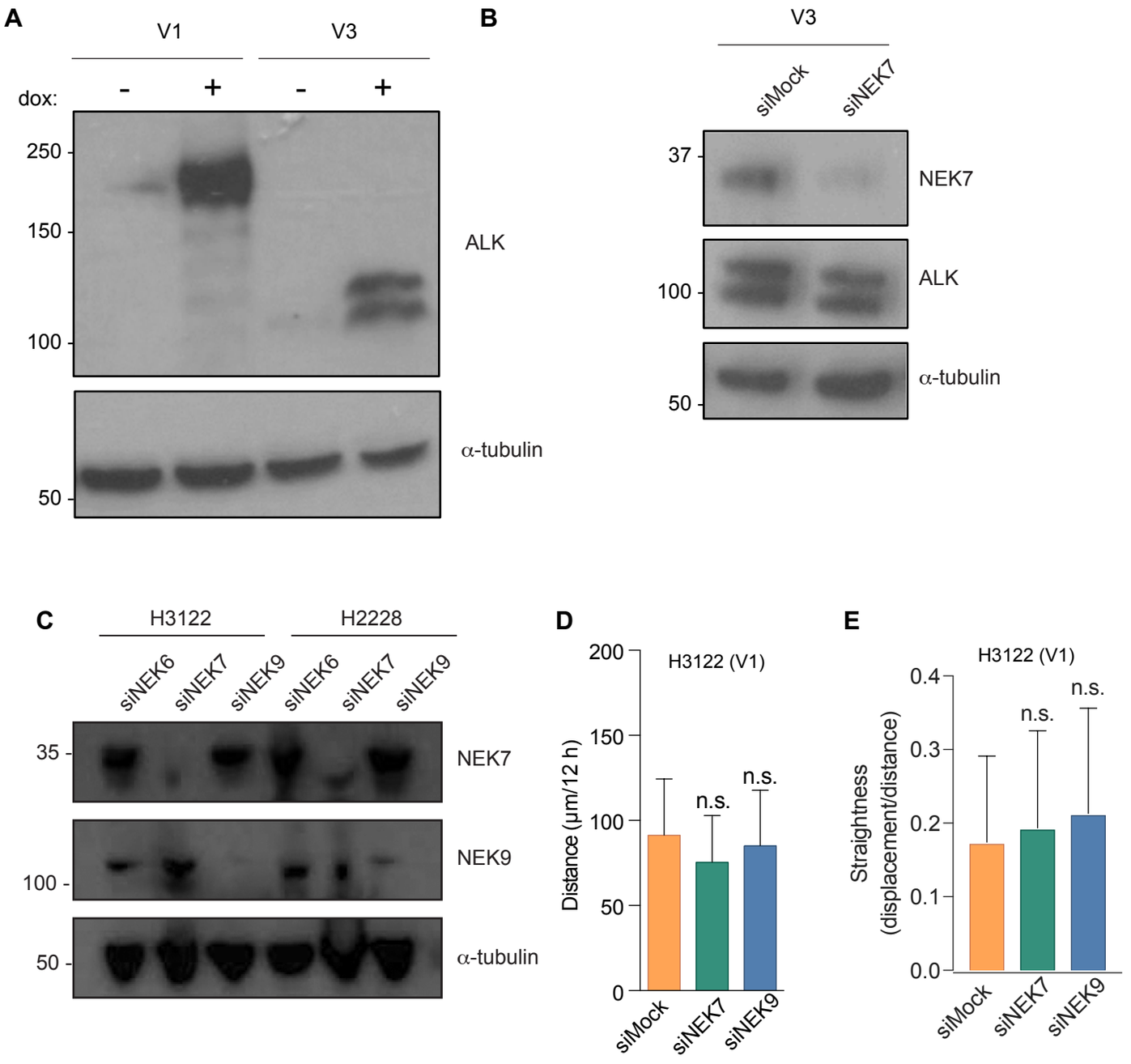

Figure S8. Validation of siRNA depletion of NEK7 and NEK9 in EML4-ALK Beas-2B and NSCLC cells

A. Beas-2B:EML4-ALK v1 or v3 U2OS were treated with doxycycline for 48 h to induce protein expression. Cell lysates were prepared and analysed by Western blot with the antibodies indicated. **B**. Beas-2B:EML4-ALK v3 cells were induced for 24 h prior to depletion for NEK7. Cell lysates were analysed by Western blot with the antibodies indicated. **C**. H3122 or H2228 cell lysates depleted for NEK6, NEK7 or NEK9 as indicated were analysed by Western blot with NEK7, NEK9 and α-tubulin antibodies. **D**. & **E**. H3122 cells that were mock, NEK7 or NEK9-depleted for 48 h were analysed by individual cell tracking. The mean distance travelled (D) and track straightness (E) is shown. M. wts (kDa) in A, B & C are indicated on the left.

Table S1. Clinicopathological characteristics of EML4-ALK NSCLC patients

182 ALK-positive patients with advanced NSCLC at Asan Medical Center (Seoul, Korea) were collected between June 2011 and August 2015. Of those, 113 patients were treated with the ALK inhibitor and had an Eastern Cooperative Oncology Group (ECOG) performance status between 0 and 3. Among 93 enrolled patients who were tissue-available and approved by the institutional review board, 38 were excluded because of poor quality of insufficient tissue samples and follow-up loss. For the analysis of the remaining 55 patients, medical records were reviewed to extract clinicopathological data including sex, age, smoking status, therapeutic agents, and survival. Of those, ALK subtyping was performed in 32 samples due to 23 cases with low quality of nucleic acid. All statistical analyses were carried out in the R software (version 3.3.3, the R Foundation for Statistical Computing, Vienna, Austria).

Parameters	*N* (%)
Sex	
Male	27 (49.1)
Female	28 (50.9)
Age in years, median (range)	54 (27 - 79)
Smoking history	
Never	37 (67.3)
≤10 pack-years	8 (14.5)
>10 pack-years	10 (18.2)
Number of previous chemotherapy	
0	38 (69.1)
1	11 (20.0)
≥ 2	6 (10.9)
Follow up in months, median (range)	15 (1 - 54)

Table S2. Clinicopathological characteristics of EML4-ALK NSCLC patients according to NEK9 expression

Based on the patients described in Supplementary Table S1, no clinicopathological characteristics exhibited a significant difference in relation to NEK9 expression. However, the number treated with previous chemotherapy was close to the borderline for significance (p=0.071) in that the proportion of patients treated with first line ALK inhibitor therapy was larger in the high Nek9 expression (score 2+/3+) group than the low expression (score 1+) group. This means that the low expression group included more intensively treated patients suggestive of more advanced NSCLC. This factor may affect the survival difference in the two groups treated with the ALK inhibitor.

Parameters - *N* (%)	Score 1+ (*N*=22)	Score 2+/3+ (*N*=33)	*P* value*
Sex			1.000
Male	11 (50)	16 (48.5)	
Female	11 (50)	17 (51.5)	
Age in years, median (range)	55 (27 - 75)	54 (37 – 76)	0.911
Smoking history			0.390
Never	14 (63.6)	23 (69.7)	
≤10 pack-years	5 (22.7)	3 (9.1)	
>10 pack-years	3 (13.6)	7 (21.2)	
Number of previous therapy			0.071
0	13 (59.1)	25 (75.8)	
1	4 (18.2)	7 (21.2)	
≥ 2	5 (22.7)	1 (3.0)	
Follow up in months, median (range)	15 (2 - 50)	15 (1 - 54)	0.486

.